1987

Thermodynamic evaluation of the Fe-Th system and glass forming ability in the Fe-Th system

Kyung Jong Lee
Iowa State University

Order Number 8805104

Thermodynamic evaluation of the Fe-Th system and glass forming ability in the Fe-Th system

Lee, Kyung Jong, Ph.D.

Iowa State University, 1987

U·M·I
300 N. Zeeb Rd.
Ann Arbor, MI 48106

Thermodynamic evaluation of the Fe-Th system and glass forming ability in the Fe-Th system

by

Kyung Jong Lee

A Dissertation Submitted to the
Graduate Faculty in Partial Fulfillment of the
Requirements for the Degree of
DOCTOR OF PHILOSOPHY

Department: Materials Science and Engineering
Major: Metallurgy

Approved:

Signature was redacted for privacy.

In Charge of Major Work

Signature was redacted for privacy.

For the Major Department

Signature was redacted for privacy.

For the Graduate College

Iowa State University
Ames, Iowa

1987

TABLE OF CONTENTS

ABSTRACT

A calculation of the Fe-Th phase relationships was undertaken in order to develop a self-consistent description of the system. A subregular solution model was used to describe the solution behavior. Intermediate phases were treated as composition invariant. Due to the limited availability of experimental thermodynamic data, a multi-step analysis was employed to develop a better description of the thermodynamic properties in the system.

As a quantitative guide to the glass forming ability (GFA) in the Fe-Th system, T_0 and TTT curves were evaluated from the previously derived thermodynamic description of the system. From the TTT curves, critical cooling rates (R_c) to avoid crystallization were determined. Since the Fe-Th system has several solid phases, the relative stability of each phase in the metastable region is discussed. Kinetic parameters such as viscosity (η), glass transition temperature (T_g) and interfacial energy (σ) were estimated since experimental values were not available.

This analysis indicates that thermodynamic data alone can not be relied upon to predict the phase boundary behavior. Both thermodynamic data and phase diagram data should be used.

OVERALL INTRODUCTION

A calculation of the Fe-Th phase relationships was undertaken in order to develop a self-consistent description of the system. A subregular solution model was used to describe the solution behavior. Intermediate phases were treated as composition invariant. Due to the limited availability of experimental thermodynamic data, a multi-step analysis was employed to develop a better description of the thermodynamic properties in the system.

First, interaction parameters for the solid and liquid solutions were evaluated by the method of Miedema et al. [1977, 1983] and Niessen et al. [1983]. Second and third, interaction parameters were calculated with invariant reactions from the phase diagram. At each step, the calculated phase diagram was compared with the evaluated one [Kubaschewski 1982].

A glass is defined as a rigid body without long range atomic order. Glass formation is controlled by a combination of thermodynamic factors, kinetic factors and processing operations [Polk and Giessen 1978]. As a quantitative guide to the glass forming ability (GFA) in the Fe-Th system, T_0 and TTT curves were evaluated from the previously derived thermodynamic description of the system. T_0 curves, which are the loci of points defining $\Delta_M G$ (solid

phase) = $\Delta_M G$ (liquid phase), are the thermodynamic limits for the partitionless crystallization of equilibrium phases. TTT curves, which result from a combined kinetic and thermodynamic approach, are time - temperature - transformation curves.

From the TTT curves, critical cooling rates (R_c) to avoid crystallization were determined. Since the Fe-Th system has several solid phases, the relative stability of each phase in the metastable region is discussed. Kinetic parameters such as viscosity (η), glass transition temperature (T_g) and interfacial energy (σ) were estimated since experimental values were not available.

PART I. THERMODYNAMIC EVALUATION OF THE FE-TH SYSTEM

INTRODUCTION

A calculation of the Fe-Th phase relationships was undertaken in order to develop a self-consistent description of the system. A subregular solution model was used to describe the solution behavior. Intermediate phases were treated as composition invariant. Due to the limited availability of experimental thermodynamic data, a multi-step analysis was employed to develop a better description of the thermodynamic properties in the system.

First, interaction parameters for the solid and liquid solutions were evaluated by the method of Miedema et al. [1977, 1983] and Niessen et al. [1983]. Second and third, interaction parameters were calculated with invariant reactions from the phase diagram. At each step, the calculated phase diagram was compared with the evaluated one [Kubaschewski 1982].

THEORY

Evaluation of the Fe-Th system

A phase diagram for the Fe-Th system was initially proposed by Thomson [1965, 1966] who studied the system over its entire range of composition at temperatures between 800°C and the liquidus. Later investigations of the crystal structures of intermediate phases were made for $Fe_{17}Th_2$ by Johnson et al. [1969], for Fe_3Th by Smith and Hansen [1965], for Fe_3Th_7 by Matthias et al. [1961] and for Fe_7Th_2 by Buschow and van der Goot [1971].

An evaluation of the composite data was made by Kubaschewski [1982] who proposed the diagram of Figure 1. The crystallography of the Th-rich and Fe-rich terminal solid solution phases and the intermediate phases has been summarized in Table 1. Lattice stabilities which are Gibbs energies of transformation as well as melting and transformation temperatures of Th and Fe were evaluated by Chase [1983] and are given in Table 2a. Gibbs formation energies of the intermediate phases in the system, shown in Table 2b, were determined by Skelton et al. [1973] at temperatures between 655°C and 891°C by an emf method. Metallographic studies by Thomson [1966] showed the solubility of Fe in Th at 950°C to be less than 2 at %. On the other side of the system, no data for the solubility of

Th in Fe have been found nor have liquidus lines been determined. Invariant reactions are summarized in Table 3.

Estimation of thermodynamic properties

Gibbs energies of mixing for terminal solid solutions of Fe in Th and Th in Fe can be expressed in the forms:

$$\Delta_M G = G_{Fe}\ (1-X_{Th}) + G_{Th}\ X_{Th} + \Delta_M G^{id} + \Delta_M G^{xs} \quad (1)$$

where:

$$\Delta_M G^{id} = RT\ ((1-X_{Th})\ln(1-X_{Th}) + X_{Th}\ln X_{Th}) \quad (2)$$

$$\Delta_M G^{xs} = X_{Th}(1-X_{Th})\ (A + B\ (2X_{Th}-1)) \quad (3)$$

X_{Th}: atomic fraction of Th

In equation (1), the first and second terms represent lattice stabilities for Fe and Th, the third term represents the ideal mixing for Fe-Th alloys, and the last term represents excess Gibbs energy of mixing.

The Gibbs energy of formation for an intermediate phase is of the form:

$$\Delta_f G = \Delta_f H - T\Delta_f S \quad (4)$$

where $\Delta_f H$ is the heat of formation and $\Delta_f S$ is the entropy of formation. To calculate the Gibbs energies which should be in agreement with proposed diagram and the available

thermodynamic measurements, a multi-step analysis has been used.

As the first step, the approach is that of Miedema [Boom et al. 1976a, 1976b] who described the heat of formation of an intermetallic compound and the heat of mixing of liquid and solid solutions with a phenomenological model. The suggested heat of mixing of a liquid solution and heat of formation of an intermetallic compound, e.g., AB alloy is

$$\Delta_M H \text{ or } \Delta_f H = 2f(C) \frac{(C_A V_A^{2/3} + C_B V_B^{2/3})}{(N_{WS}^A)^{-1/3} + (N_{WS}^B)^{-1/3}} * (-P(\Delta\phi^*)^2 + Q(\Delta N_{WS}^{1/3})^2 - R) \quad (5)$$

where:

$f(C) = C_A^S C_B^S$ for a liquid solution

$= C_A^S C_B^S (1 + 8(C_A^S C_B^S)^2)$ for an intermetallic compound

$$C_A^S = \frac{C_A V_A^{2/3}}{(C_A V_A^{2/3} + C_B V_B^{2/3})}$$

C: atomic concentration (# of atoms/ cm^3)

N_{WS}: density of electrons at the boundary between dissimilar atomic cells

ϕ^*: chemical potential for electrons

V_i: molar volume of the subscribed element

P, Q and R: the coefficients dependent on types of

binary alloy systems

The first term takes cognizance of the chemical potential difference between the two atomic species and represents an energy reduction of the heat of mixing due to electron transfer to the more electropositive species. The second term is the positive energy cost of eliminating the electronic density discontinuity at the boundaries of Wigner-Seitz cells. The last term is an energy reduction attributable to hybridization of d-p electron bands.

In alloying, there is a volume change due to the charge transfer. The molar volume change is

$$V_A^{2/3}\ (\text{alloy}) = V_A^{2/3}\ (\text{pure})\ (1 + \text{acf}\ C_B^S(\phi_A^* - \phi_B^*)) \qquad (6)$$

where acf is a constant that has been empirically determined from experimental data to be 0.14, 0.10, 0.07 and 0.04 for monovalent, divalent, trivalent and higher valent metals. To calculate the heat of formation, the volume of alloy per mole of atoms rather than that of either element was used.

For a solid solution, the heat of alloy formation is

$$\Delta_M H(\text{solid solution}) = \Delta_M H(\text{liquid solution}) + \Delta_M H(\text{elastic energy}) + \Delta_M H(\text{structure energy}) \qquad (7)$$

Here the second term arising from elastic mismatch can be estimated [Eshelby 1954, Friedel 1954] from elastic continuum theory. Thus, $\Delta_M H$ (elastic energy) in A-B alloy may be expressed as follows:

$$\Delta_M H(\text{elastic energy}) = X_A X_B (X_A \Delta_M H_{A \text{ in } B}^{\text{elastic}} + X_B \Delta_M H_{B \text{ in } A}^{\text{elastic}}) \quad (8)$$

where

$$\Delta_M H_{A \text{ in } B}^{\text{elastic}} = 2\mu_B \frac{3K_A}{3K_A + 4\mu_B} \frac{(\Delta V_{AB})^2}{3V_A} \quad (9)$$

where μ_B is the shear modulus of the B element, K_A is the bulk modulus of the A element and ΔV_{AB} is the difference in molar volume of the two metals. The third term in equation (7) accounts for the preference for a certain crystal structure in transition metal alloy systems. This term was summarized by Miedema using theoretical estimates for the difference in energy for pure transition metals with the average number of conduction electrons per atom (Z) [Pettifor 1977] and experimental information about solid solubilities and enthalpy differences between crystal structures. $\Delta_M H$ (structure energy) can be expressed:

$$\Delta_M H(\text{structure}) = X_A X_B (X_A \Delta_M H_{A \text{ in } B}^{\text{structure}} + X_B \Delta_M H_{B \text{ in } A}^{\text{structure}}) \quad (10)$$

where

$$\Delta_M H_{A \text{ in } B}^{\text{structure}} = -E_A(\phi_A) + E_B(\phi_B) + (Z_A - Z_B)\left(\frac{dE_B(\phi_B)}{dZ}\right) \quad (11)$$

where A and B are elements, ϕ_i is the phase and E_i is the structure dependent energy of the subscripted element. E and dE/dZ, shown in Table 4 and Table 5, were summarized by Miedema and Niessen [1983].

Use of invariant reactions

As the second and third step, invariant reactions were used to optimize the interaction parameters of solution phases and Gibbs energies of formation for intermediate phases.

For example, from the 875°C temperature of the eutectic reaction (Liquid (55 at.% Th) -> Fe_3Th + Fe_3Th_7) and the equilibrium requirement of equality of the partial molar Gibbs energies, which are,

$$\Delta_M \bar{G}_i^L = \Delta_f \bar{G}_i^{Fe_3Th} = \Delta_f \bar{G}_i^{Fe_3Th_7} \qquad (i: \text{ Fe or Th}) \quad (12)$$

the following two equations were derived.

$$\Delta_M G^L \ (X_{Th}=0.55, 1148K) = \left(\frac{d\Delta_M G^L}{dX_{Th}}\right) \ (X_{Th}=0.55, 1148K)$$
$$(0.55-0.25) + \Delta_f G^{Fe_3Th_7}(1148K) \quad (13)$$

$$\frac{d\Delta_M G^L}{dX_{Th}} (X_{Th}=0.55, 1148K) = \frac{\Delta_f G^{Fe_3Th}(1148K) - \Delta_f G^{Fe_3Th_7}(1148K)}{0.25 - 0.7} \quad (14)$$

With the following equations for $\Delta_f G^{Fe_3Th_7}(T)$, $\Delta_f G^{Fe_3Th}(T)$, $\Delta_M G^L(T, X_{Th})$ and $d\Delta_M G^L/dX_{Th}(T, X_{Th})$, interaction parameters (A and B) for the liquid phase can be evaluated.

$$\Delta_M G^{Fe_3Th_7}(T) = -5021-1.67T \quad (15)$$

$$\Delta_M G^{Fe_3Th}(T) = -24769+12.55T \quad (16)$$

$$\Delta_M G^L(T, X_{Th}) = (17406-9.029T)X_{Th} + (15540-8.8976T)(1-X_{Th}) + RT(X_{Th}\ln X_{Th} + (1-X_{Th})\ln(1-X_{Th})) + X_{Th}(1-X_{Th})(A + B(2X_{Th}-1)) \quad (17)$$

$$(d\Delta_M G^L/dX_{Th})(T, X_{Th}) = (17406-9.029T) - (15540-8.8976T) + RT(\ln X_{Th} - \ln(1-X_{Th})) + 2B\, X_{Th}(1-X_{Th}) + (1-2X_{Th})(A + B(2X_{Th}-1)) \quad (18)$$

This can be accomplished by substituting equations (15)-(18) into (13) and (14) with T=1148 K and X_{Th}=0.55 to generate A= -31604 J/mol and B= 1684 J/mol.

In similar manner values from invariant reactions in Table 3 were used to optimize the interaction parameters of other solution phases and unavailable high temperature

Gibbs formation energies of intermediate phases after initially using Miedema approach to develop first approximations.

RESULTS AND DISCUSSION

As the first step $\Delta_M G^{XS}$ values for liquid and solid solution phases were calculated by the Miedema approach with constraints from the known invariant reactions. Throughout the calculation, αFe(bcc) and αTh(fcc) were used as standard states. $\Delta_M G^{XS}$ was expressed with a subregular solution model, which is,

$$\Delta_M G^{XS} = X_{Th}(1-X_{Th})\ (A + B\ (2X_{Th}-1)) \qquad (19)$$

The data in Table 12 were substituted into equation (5) to calculate the heat of mixing of a liquid solution. The values of P, Q and R in Table 12 are empirical constants that were determined by Miedema for transition metal alloy systems [Boom et al. 1976a, 1976b].

The constants in equation (5) for the liquid solution were evaluated as A= -42739 J/mol and B= 11756 J/mol. For the solid solution phases, the structure dependent energy and the elastic strain energy terms were calculated by substituting data from Table 13 into equations (7), (9) and (11).

This produced the following values for the excess Gibbs energies of phase formation.

$$\Delta_M G^{xs}_{bcc}(\text{structure E}) = X_{Th}(1-X_{Th})(-36000 + 20000(2X_{Th}- 1)) \quad (20)$$

$$\Delta_M G^{xs}_{fcc}(\text{structure E}) = X_{Th}(1-X_{Th})(32000 - 20000(2X_{Th}- 1)) \quad (21)$$

$$\Delta_M G^{xs}(\text{strain E}) = X_{Th}(1-X_{Th})(246000- 99000(2X_{Th}- 1)) \quad (22)$$

Total excess Gibbs energies for fcc and bcc phases were

$$\Delta_M G^{xs}_{bcc} = X_{Th}(1-X_{Th}) (167000-67000(2X_{Th}-1)) \quad (23)$$

$$\Delta_M G^{xs}_{fcc} = X_{Th}(1-X_{Th}) (235000-107000(2X_{Th}-1)) \quad (24)$$

For the intermediate phases, experimentally measured heats of formation were used. Derived Gibbs energies of all phases were summarized in Table 6. A calculated phase diagram from Table 6 was shown in Figure 2.

Calculated liquidus lines at the Th-rich side were in good agreement with the evaluate ones (Figure 1). However at the Fe-rich side, experimental liquidus lines were depressed by 100 - 200°C compared to calculated ones. This resulted from the fact that the stability of $Fe_{17}Th_2$ was too low with respect to the stability of liquid phase to show a eutectic reaction (L -> δFe + $Fe_{17}Th_2$).

Moreover, compound phases showed low stabilities such that several peritectic reactions occurred at temperatures lower than expected.

In a second step, recalculation of parameters was carried out to optimize the Gibbs energies using invariant reactions and equilibrium conditions. Calculated results are listed in Table 7. Equations (4) and (5) from Table 7 were used to evaluate interaction parameters (A and B) for the formation of liquid solution. This was possible because $\Delta_f G^{Fe_3Th}$ (1148 K) and $\Delta_f G^{Fe_3Th_7}$ (1235 K) were experimentally available. The bcc and fcc solid phases were treated as regular solutions and their interaction parameters (C and D) were generated from equations (7) and (8) of Table 7. The entropy of formation of $Fe_{17}Th_2$ ($\Delta_f S^{Fe_{17}Th_2}$) was taken from equation (9) in Table 7. The optimization was done by linear regression. Resulting values for A, B, C, D and $\Delta_f S^{Fe_{17}Th_2}$ were -32000 J/mol, 2000J/mol, 30000J/mol, 30000 J/mol and -2.274 J/mol deg. Calculated parameters in the second step are given in Table 8. The phase diagram is shown in Figure 3. The diagram is in good agreement with the evaluated one except that the peritectic reactions involving Fe_5Th and Fe_3Th occurred at lower temperature than expected and that Fe_7Th_2 phase was disappeared in the calculated diagram.

The last step was the evaluation of the Gibbs energies

of formation of the intermediate phases. Since the experimental measurements of Gibbs energies of formation for intermediate phases were done at temperatures between 655 and 891°C which is well below the temperatures of most of the invariant reactions in the system, and because the temperature dependence of those Gibbs energies are more uncertain than the magnitude, extrapolation upward into the temperature regimes of the invariant reactions has a large inherent uncertainty. Values for $\Delta_f H$ and $\Delta_f S$ of the intermediate phases were therefore modified to retain consistency with the evaluated interaction parameters of the liquid and solid solution phases while remaining consistent with $\Delta_f G$'s in the temperature range of measurement. Equations (1) to (6) and (9) to (11) in Table 7 were used to calculate the Gibbs energies of formation for the intermediate phases.

For example, to get the $\Delta_f G^{Fe_5Th}$, the regression method was used with following equations.

$$\Delta_f G^{Fe_5Th}\ (T) = -19205 + 8.835T \quad (928\ K < T < 1164\ K) \qquad (25)$$

$$\Delta_f G^{Fe_5Th}\ (1485\ K) = -8201 \qquad (26)$$

$$\Delta_f G^{Fe_5Th}\ (1473\ K) = -8636 \qquad (27)$$

where unit is J/mol.

As a result, $\Delta_f G^{Fe_5Th}(T) = -14996 + 4.57T$ was

derived. The Gibbs energies of formation for the intermediate phases that were derived by the regression method are listed in Table 9. Final parameters defining the Gibbs energies of formation for the various phases are given in Table 10 and the phase diagram that was calculated from these parameters is shown in Figure 4. Comparison of calculated and experimental diagrams is done by the superposition in Figure 5.

The interaction parameters of the liquid phase combined to approach -30 kJ/mol for the heat of solution of Fe in Th at infinite dilution and -34 kJ/mol for the heat of solution of Th in Fe at infinite dilution. Refined heats of formation of compound phase are compared with those from experiment and from the Miedema approximation in Table 11.

SUMMARY AND CONCLUSIONS

It was not the purpose of this study to reevaluate the phase diagram, but rather to generate internally consistent thermodynamics functions for each phase. From the phase diagram information, mostly invariant reactions, experimental data and a theoretical model, such thermodynamic descriptions for the phases were obtained with input information. First, all available thermodynamic data were assembled and a model which satisfactorily fits the experimental data was developed. Since any regression creates a best fit to all data, parameters were reevaluated such that they predicted certain critical phase diagram areas exactly along with representing the thermodynamic property. The second and third step in this study was set up in a way that each step optimized the parameters such that the difference between evaluated phase diagram and calculated one is approximately zero.

This analysis indicates that thermodynamic data alone can not be relied upon to predict the phase boundary behavior. Both thermodynamic data and phase diagram data should be used.

Table 1. Crystal Structure in the Fe-Th System

Phase	Proto type	Pearson Symbol	Space Group
αTh	Cu	cF4	$Fm\bar{3}m$
γFe	Cu	cF4	$Fm\bar{3}m$
βTh	W	cI2	$Im\bar{3}m$
δFe	W	cI2	$Im\bar{3}m$
αFe	W	cI2	$Im\bar{3}m$
$Fe_{17}Th_2$	$Fe_{17}Th_2$	hR19	$R\bar{3}m$
Fe_5Th	$CaCu_5$	hP6	P6/mmm
αFe_7Th_2	Ce_2Ni_7	hP36	$P6_3/mmc$
βFe_7Th_2	Gd_2Co_7	(rhombohedral)	————
Fe_3Th	$NbBe_3$	hR12	$R\bar{3}m$
Fe_3Th_7	Fe_3Th_7	hP20	$P6_3mc$

Table 2a. Lattice Stability of Fe and Th

Element	$\Delta_M G$ (J/mol)	Transformation Temperature (°C)
Th (α-β)	3600-2.2T	1360
(β-L)	13800-6.8T	1735
(α-L)	17400-9.0T	1660
Fe (α-γ)	900-0.76T	911
(γ-δ)	840-0.50T	1392
(δ-L)	13800-7.63T	1536
(γ-L)	14640-8.13T	1528
(α-L)	15540-8.89T	1475

Table 2b. Gibbs Formation Energies of Intermediate Phases[a]

Phase	$\Delta_f G$ (J/mol)	Temperature Range (°C)
$Fe_{17}Th_2$	-12468+4.98T	(655 - 891)
Fe_5Th	-19205+8.835T	(655 - 891)
Fe_7Th_2	-22845+11.21T	(655 - 891)
Fe_3Th	-24769+12.55T	(655 - 891)
Fe_3Th_7	-5021-1.67T	(655 - 891)

[a]Compound reaction $xFe(\alpha)+(1-x)Th(\alpha) \rightarrow Fe_xTh_{1-x}$.

Table 3. Special Reactions of the Fe-Th System

Reaction	Compositions (at.% Th)			Temp. (°C)	Reaction Type
$Fe_{17}Th_2(L) \rightarrow Fe_{17}Th_2$		10.53		1462	Congruent
$L \rightarrow \delta Fe + Fe_{17}Th_2$	6.0	0	10.53	1412	Eutectic
$L+Fe17Th2 \rightarrow Fe_5Th$	26	10.53	16.7	1212	Peritectic
$L+Fe_5Th \rightarrow Fe_3Th$	30	16.7	25	1200	Peritectic
$L \rightarrow Fe_3Th+Fe_3Th_7$	55	25	70	875	Eutectic
$L+\alpha Th \rightarrow Fe_3Th_7$	67.5	99	70	962	Peritectic
$Fe_5Th+Fe_3Th \rightarrow Fe_7Th_2$	16.7	25	22.22	----	Peritectoid

Table 4. Enthalpy Differences between hcp, bcc and fcc Phases[a]

Z	3	4	5	5.5	6	7	8	8.5	9	10
hcp	-2.5	-2.5	10	15	13	-5	-10.5	-11	-8	-1
fcc	-2	-1.5	9	14	11	-3	-9.5	-11	-9	-2
bcc	2.2	2	-9.5	-14.5	-12	4	10	11	8.5	1.5

[a]Unit: KJ/mol.

Table 5. Change of the Structure Dependent Energy with the Average Number of Valence Electrons per Atom (i.e., dE/dZ)[a]

Z		3	4	5	6	7	8	9	10
hcp	Z<0	-	0	13	-4	-18	-6	6	7
	Z>0	0	13	10	-18	-6	-1	7	-
fcc	Z<0	-	1	11	-6	-14	-7	4	7
	Z>0	1	11	10	-14	-7	-3	7	-
bcc	Z<0	-	0	-12	5	16	6	-5	-7
	Z>0	0	-12	-10	16	-6	2	-7	-

[a]Unit: KJ/mol per electron.

Table 6. Gibbs Energies Determined from Step 1 (Miedema model)[a]

Phase	$\Delta_M G_{Th}$	$\Delta_M G_{Fe}$	A	B
bcc1(α)	3599-2.204T	0	167000	-67000
bcc2(δ)	3599-2.204T	1740-1.2646T	167000	-67000
fcc	0	900-0.7061T	235000	-107000
liquid	17406-9.029T	15540-8.8976T	-42739	11756
Fe_3Th_7	-	-	-5021	1.67
Fe_3Th	-	-	-24769	-12.55
Fe_7Th_2	-	-	-22845	-11.21
Fe_5Th	-	-	-19205	-8.835
$Fe_{17}Th_2$	-	-	-12468	-4.98

[a]For solution phases: $\Delta_M G^{xs}=X_{Th}(1-X_{Th})(A+B\ (2X_{Th}-1))$; for solid intermediate phases: $\Delta_f G = A - BT$.

Table 7. Thermodynamic Information from Invariant Reactions[a]

$\Delta_f G^{Fe_5Th}$ (1485) = $(d\Delta_M G^L/dX_{Th})$ (1485, 0.26) (0.1667-0.26) + $\Delta_M G^L$ (1485, 0.26)	(1)
$\Delta_f G^{Fe_5Th}$ (1473) = $(d\Delta_M G^L/dX_{Th})$ (1473, 0.3) (0.1667-0.3) + $\Delta_M G^L$ (1473, 0.3)	(2)
$\Delta_f G^{Fe_3Th}$ (1473) = $(d\Delta_M G^L/dX_{Th})$ (1473, 0.3) (0.25 -0.3) + $\Delta_M G^L$ (1473, 0.3)	(3)
$\Delta_f G^{Fe_3Th}$ (1148) = $(d\Delta_M G^L/dX_{Th})$ (1148, 0.55) (0.25 -0.55) + $\Delta_M G^L$ (1148, 0.55)	(4)
$\Delta_f G^{Fe_3Th_7}$ (1148) = $(d\Delta_M G^L/dX_{Th})$ (1148, 0.55) (0.7 - 0.55) + $\Delta_M G^L$ (1148, 0.55)	(5)
$\Delta_f G^{Fe_3Th_7}$ (1235) = $(d\Delta_M G^L/dX_{Th})$ (1235, 0.675) (0.7 -0.675) + $\Delta_M G^L$ (1235, 0.675)	(6)
$\Delta_M G^{fcc}$ (1235, 0.99) = $(d\Delta_M G^L/dX_{Th})$ (1235, 0.675) (0.7 -0.675) + $\Delta_M G^L$ (1235, 0.675)	(7)
$\Delta_M G^{bcc}$ (1685, 0.0) = $(d\Delta_M G^L/dX_{Th})$ (1685, 0.1053) (0- 0.1053) + $\Delta_M G^L$ (1685, 0.1053)	(8)
$\Delta_f G^{Fe_{17}Th_2}$ (1735) = $(d\Delta_M G^L/dX_{Th})$ (1735, 0.1053) (0) + $\Delta_M G^L$ (1735, 0.1053)	(9)

[a] G(T(K), mole fraction of Th).

Table 7. (Continued)

$$\Delta_f G^{Fe_{17}Th_2}(1685) = (d\Delta_M G^L/dX_{Th})(1685,0.06)(0.1053 - 0.06) + \Delta_M G^L(1685,0.06) \quad (10)$$

$$\Delta_f G^{Fe_{17}Th_2}(1485) = (d\Delta_M G^L/dX_{Th})(1485,0.26)(0.1053 - 0.26) + \Delta_M G^L(1485,0.26) \quad (11)$$

Table 8. Gibbs Energies of Formation Determined by Invariant Reaction (Step 2)[a]

Phase	$\Delta_M G_{Th}$	$\Delta_M G_{Fe}$	A	B
bcc1(α)	3599-2.204T	0	30000	0
bcc2(δ)	3599-2.204T	1740-1.2646T	30000	0
fcc	0	900-0.7061T	30000	0
liquid	17406-9.029T	15540-8.8976T	-32000	2000
Fe_3Th_7	-	-	-5021	1.67
Fe_3Th	-	-	-24769	-12.55
Fe_7Th_2	-	-	-22845	-11.21
Fe_5Th	-	-	-19205	-8.835
$Fe_{17}Th_2$	-	-	-12468	-2.274

[a]For solution phases: $\Delta_M G^{xs}=X_{Th}(1-X_{Th})(A+B\ (2X_{Th}-1))$; for solid intermediate phases: $\Delta_f G = A - BT$.

Table 9. Gibbs Energies of Formation used in Last Step

Phase	$\Delta_f G$(J/mol)	Temp. Range (K)
Fe_5Th	-19205 + 8.835T	928< T < 1164
	-8021	1485
	-8636	1473
$Fe_{17}Th_2$	-12468 + 4.98T	928 < T < 1164
	-7743	1735
	-7444	1685
	-6587	1485
Fe_3Th_7	-5021 - 1.67T	928 < T < 1164
	-7113	1235
	-6999	1148
Fe_3Th	-24769 + 12.55T	928 < T < 1164
	-10384	1473
	-10509	1148

Table 10. Gibbs Energies Determined from Last Step[a]

Phase	$\Delta_M G_{Th}$	$\Delta_M G_{Fe}$	A	B
bcc1(α)	3599-2.204T	0	30000	0
bcc2(δ)	3599-2.204T	1740-1.2646T	30000	0
fcc	0	900-0.7061T	30000	0
liquid	17406-9.029T	15540-8.8976T	-32000	2000
Fe_3Th_7	-	-	-4961	1.74
Fe_3Th	-	-	-17311	-5.33
Fe_7Th_2	-	-	-22845	-11.21
Fe_5Th	-	-	-14996	-4.57
$Fe_{17}Th_2$	-	-	-7953	-0.181

[a]For solution phases: $\Delta_M G^{xs}=X_{Th}(1-X_{Th})(A+B\ (2X_{Th}-1))$; for solid intermediate phases: $\Delta_f G = A - BT$.

Table 11. Comparison of the Heats of Formation for Compound Phases

Phase	Experimental	Miedema Model	Last step (Regressed)
$Fe_{17}Th_2$	-12468	-5824	-7953
Fe_5Th	-19205	-9177	-14996
Fe_7Th_2	-22845	-11852	-22845
Fe_3Th	-24769	-12978	-17311
Fe_3Th_7	-5021	-9461	-4961

Table 12. Values for the Molar Volume, the Density of Electrons, the Chemical Potential for Electron and acf

	$V(cm^3/mol)$	$N_{ws}^{1/3}$ $(du^{1/3})^*$	$\phi^*(V)$	acf
Fe	7.094	1.77	4.93	0.04
Th	19.79	1.28	3.30	0.04

$P = 0.147$ eV $/(V^2 cm^2 du^{1/3})$

$Q = 9.4$ eV $/(du\ cm^2)$

$R = 0$ eV $/(du^{1/3} cm^2)$

where $1eV = 1.602 * 10^{-19}$ J

du(density unit) = 100 $kg^{1/2} cm^{-5/2}$

du is defined as $(K/V)^{1/2}$.

Table 13. Parameters used in equation (7)

	electronic structure	Z	V (cm^3/mol)	$\mu * 10^{-6}$ (kg/cm^2)	$K * 10^{-6}$ (kg/cm^2)
Fe	$3d^6 4s^2$	8	7.094	0.831	1.716
Th	$6d^2 7s^2$	4	19.79	0.284	0.5534

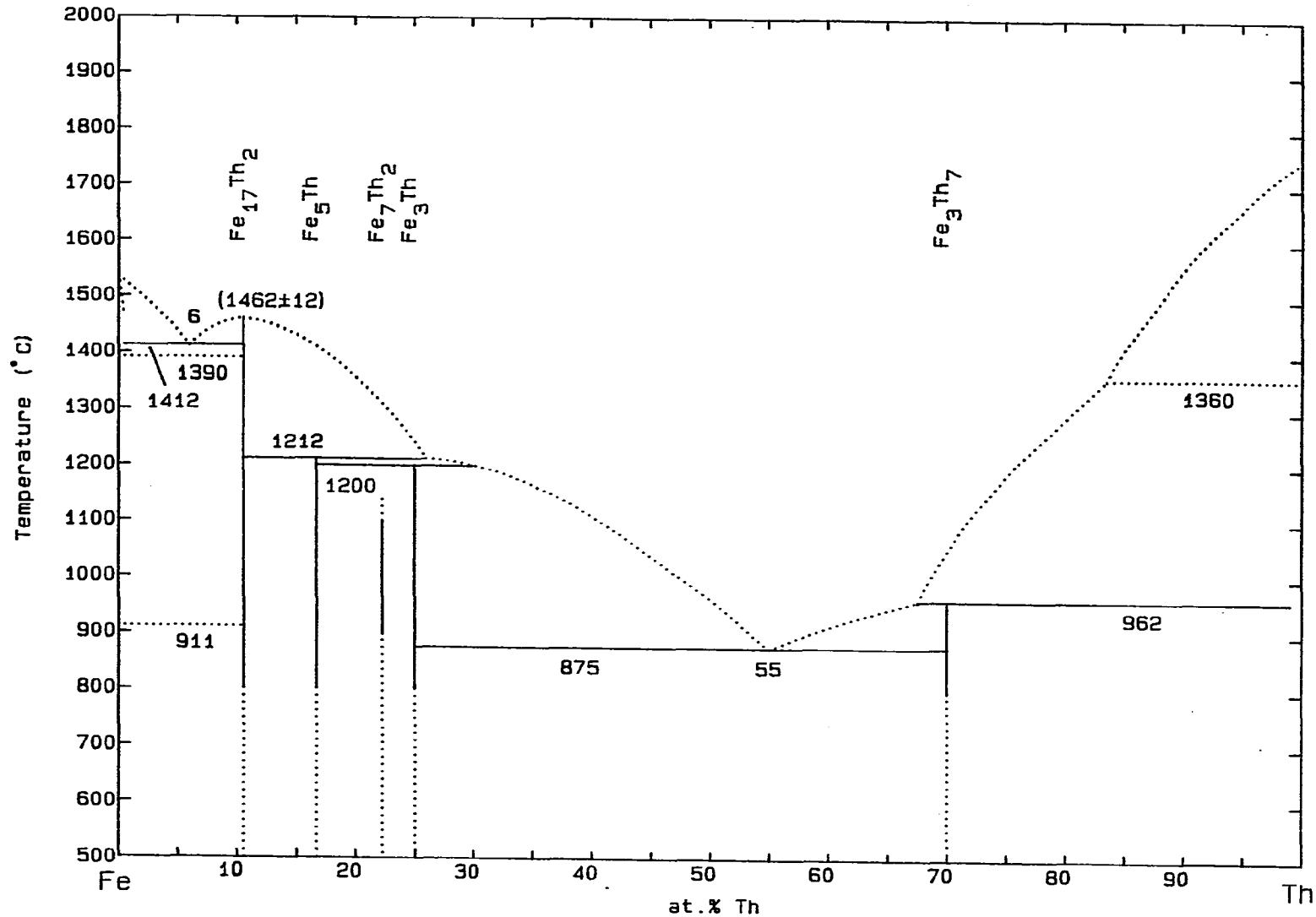

Fig. 1 The Fe-Th system evaluated from experiment

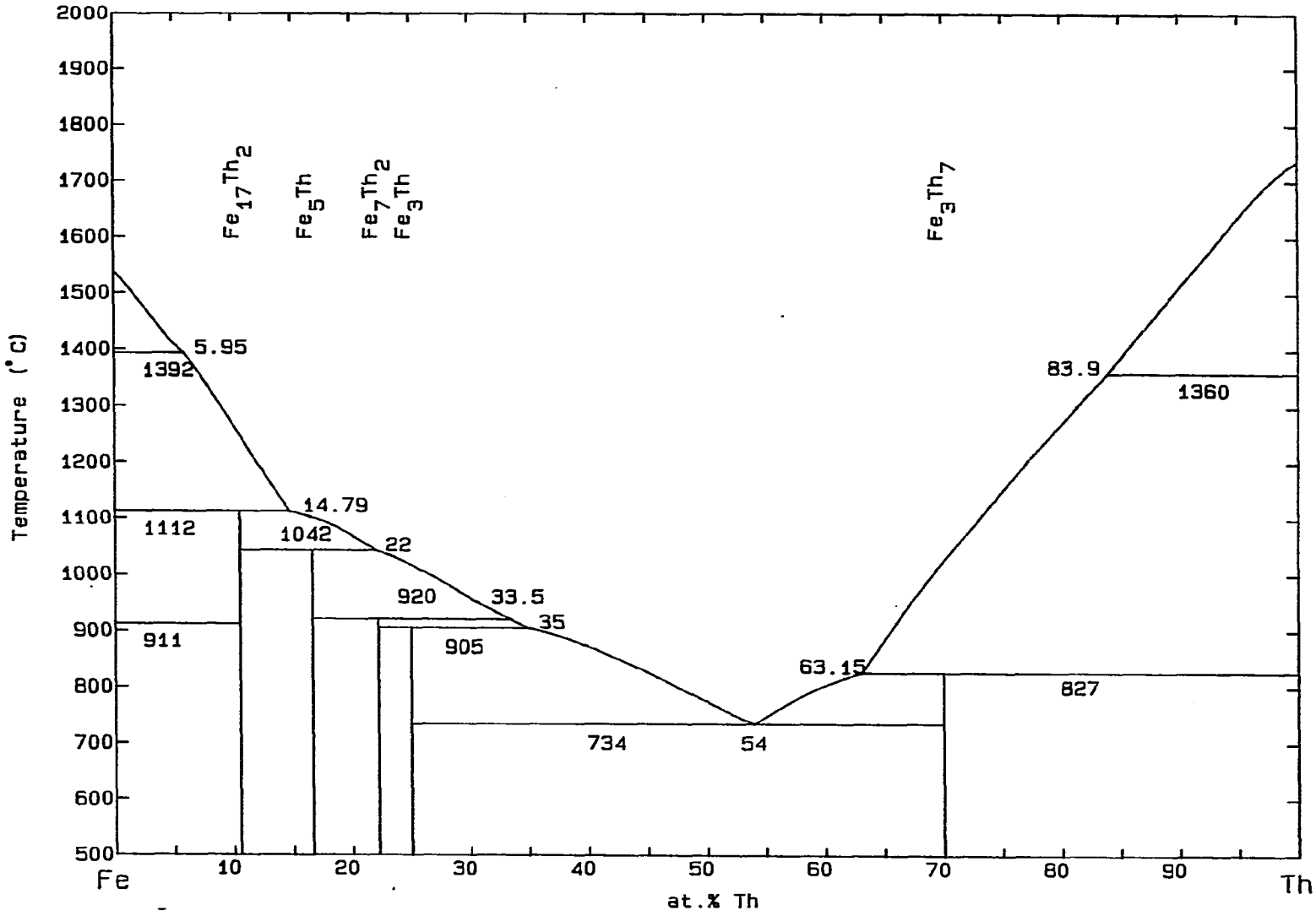

Fig. 2 The Fe-Th system (Miedema approximation)

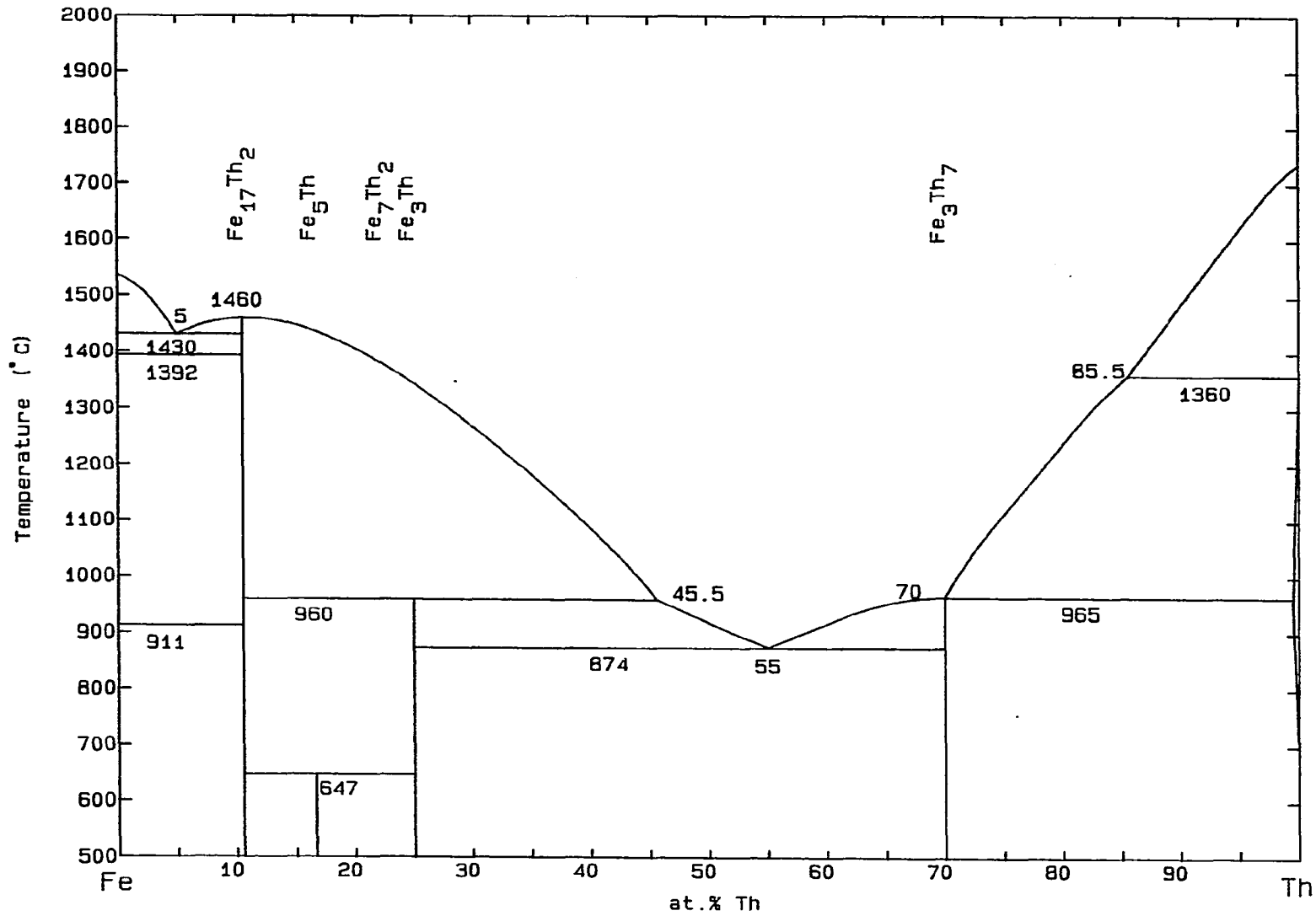

Fig. 3 The Fe-Th system (Second step analysis)

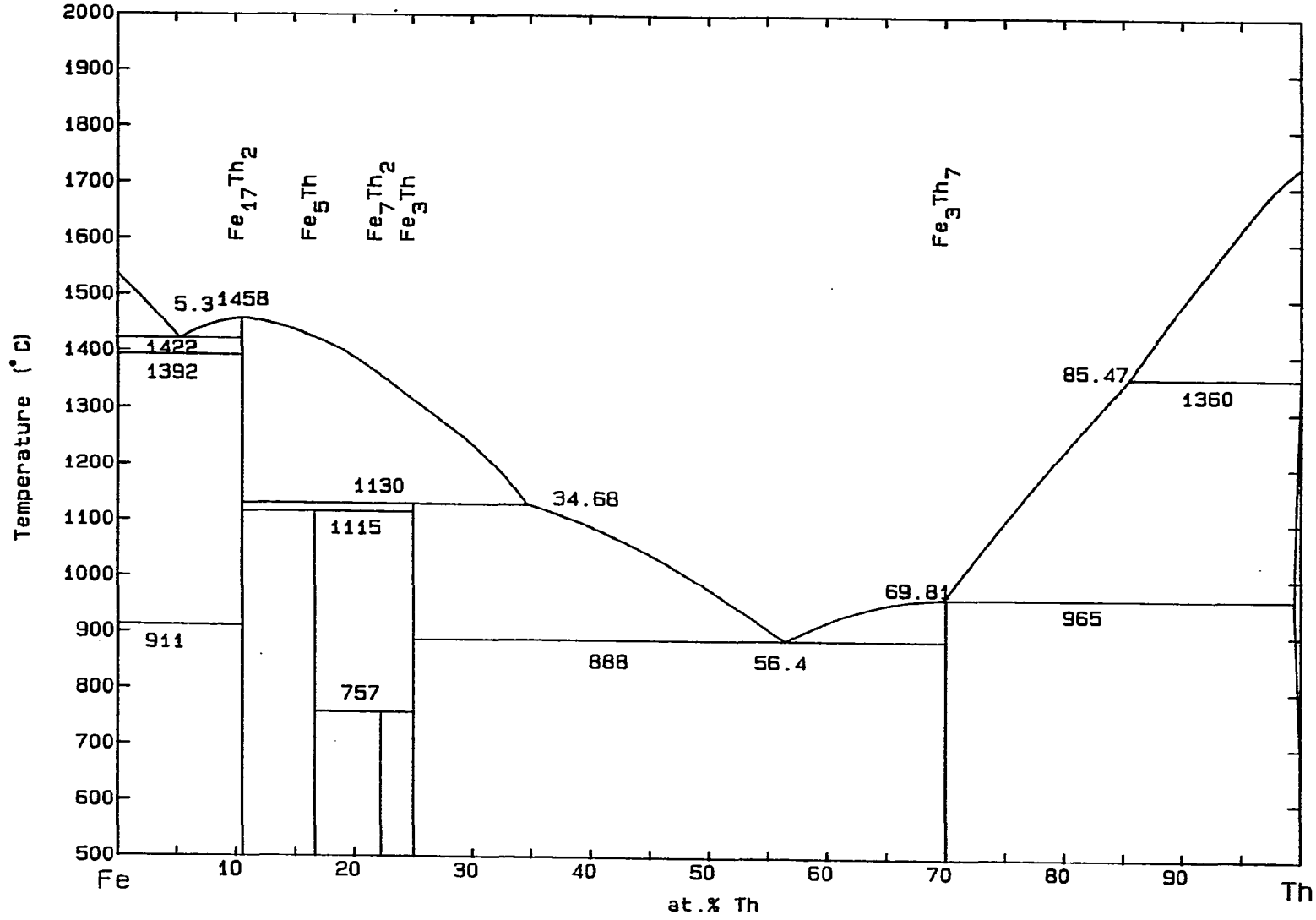

Fig. 4 The Fe-Th system (Last step analysis)

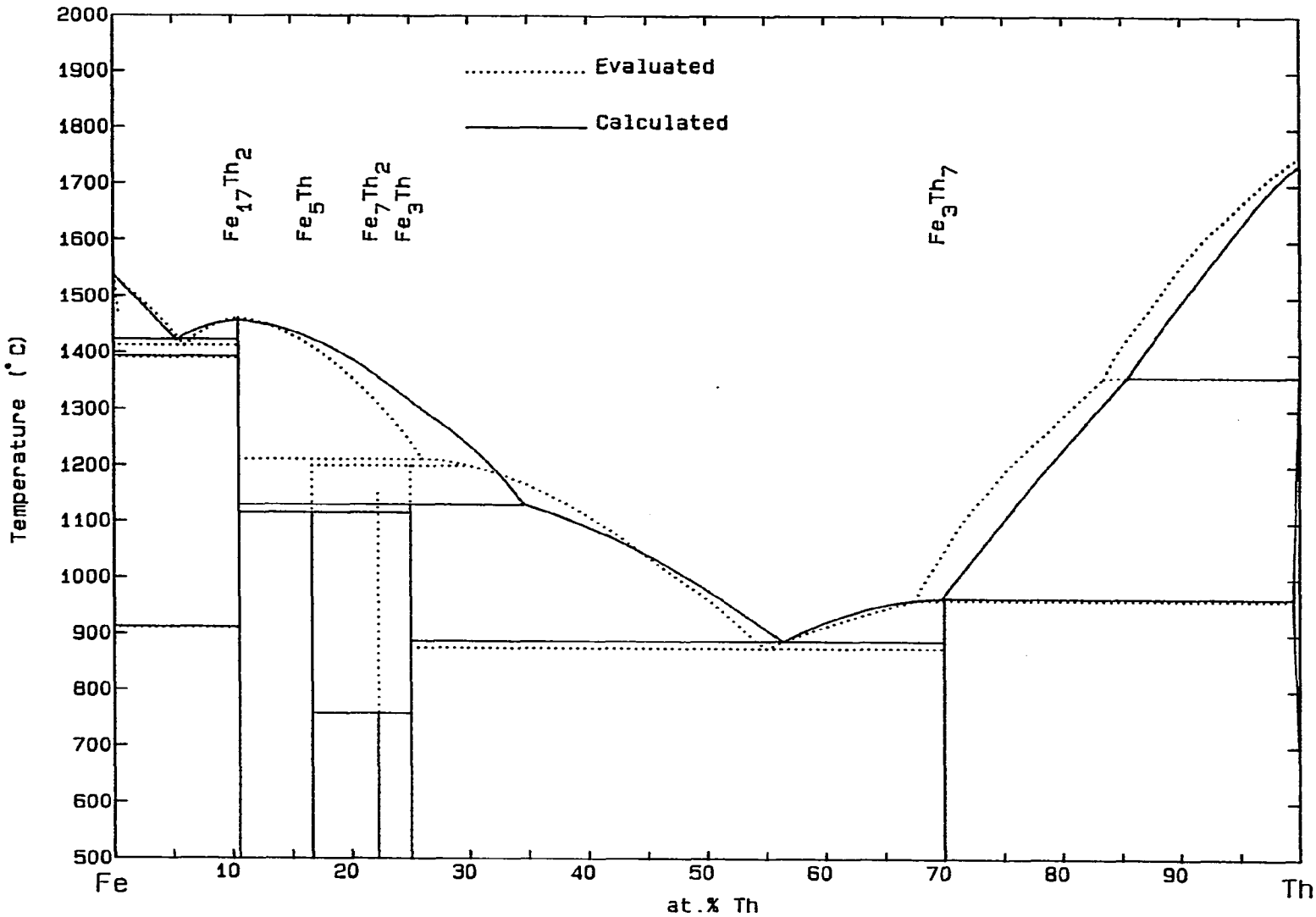

Fig. 5 The Fe-Th system (Comparison)

REFERENCES

Boom R., F. R. De Boer and A. R. Miedema, J. Less Common Met., 45, 237 (1976a)

Boom R., F. R. De Boer and A. R. Miedema, J. Less Common Met., 46, 271 (1976b)

Buschow K. H. J. and A. S. van der Goot, J. Less Common Met., 23, 399 (1971)

Chase W. M., Bull. of Alloy Phase Diagrams, 4, 124 (1983)

Eshelby D. J., J. Appl. Phys., 25, 255 (1954)

Friedel J., Advances in Physics, 3, 446 (1954)

Johnson Q., G. S. Smith and D. H. Wood, Acta Crystallogr., B25, 464 (1969)

Kubaschewski O., Iron Binary Phase Diagrams, Spring-Verlag, Berlin (1982)

Matthias B. T., V. B. Compton and E. Corenzwit, Phys. Chem. Solids, 19, 130 (1961)

Miedema A. R., F. R. De Boer, R. Boom and J. W. F. Dorleijn, Calphad, 11, 341 (1977)

Miedema A. R. and A. K. Niessen, Calphad, 7, 27 (1983)

Niessen A. K., F. R. De Boer, R. Boom, P. F. De Chatel, W. C. M. Mattens and A. R. Miedema, Calphad, 7, 51 (1983)

Pettifor D. G., Calphad, 1, 305 (1977)

Skelton W. M., N. J. Magnani, J. F. Smith, Met. Trans. 4, 917 (1973)

Smith J. F. and D. H. Hansen, Acta Crystallogr., 19, 879 (1965)

Thomson J. R., J. Nucl. Mater., 15, 88 (1965)

Thomson J. R., J. Less Common Met., 10, 432 (1966)

PART II. GLASS FORMING ABILITY IN THE FE-TH SYSTEM

INTRODUCTION

A glass is defined as a rigid body without long range atomic order. Glass formation is controlled by a combination of thermodynamic factors, kinetic factors and processing operations [Polk and Giessen 1978]. As a quantitative guide to the glass forming ability (GFA) in the Fe-Th system, T_0 and TTT curves were evaluated from the previously derived thermodynamic description of the system. T_0 curves, which are the loci of points defining $\Delta_M G$(solid phase) = $\Delta_M G$(liquid phase), are the thermodynamic limits for the partitionless crystallization of equilibrium phases. TTT curves, which result from a combined kinetic and thermodynamic approach, are time-temperature-transformation curves.

From the TTT curves, critical cooling rates (R_c) to avoid crystallization were determined. Since the Fe-Th system has several solid phases, the relative stability of each phase in the metastable region is discussed. Kinetic parameters such as viscosity(η), glass transition temperature (T_g) and interfacial energy (σ) were estimated since experimental values were not available.

THEORY

The determinations of T_0 curves were carried out using the thermodynamic functions for the liquid phase and the terminal solid phases. T_0 curves for intermediate phases were not determined because those phases were treated as invariant in composition.

To calculate the TTT curves, the Johnson-Mehl-Avrami treatment [Christian 1965] was used. According to their approach the crystallized volume fraction (x_f) is

$$x_f = \frac{\pi}{3} I_v U_c^3 t^4 \qquad (1)$$

where

x_f: the transformed volume fraction

I_v: the nucleation frequency

U_c: the growth rate

t: the time required to transform to solid

Nucleation was assumed to be homogeneous since glass transformation occurs when the cooling rate is high. The homogeneous nucleation frequency is

$$I_v = \frac{D_n N_v}{a_0} \exp\left(-\frac{\Delta_M G^*(T,X)}{kT}\right) \qquad (2)$$

where

D_n = the diffusion coefficient of liquid controlling nucleation

N_v = the number of atoms per unit volume

a_0 = an atomic diameter

$\Delta_M G^*(T,X)$ = the Gibbs energy barrier for nucleation

By classical nucleation theory, $\Delta_M G^*(T,X)$ is expressed as

$$\Delta_M G^* = \frac{16\pi}{3N_a} \frac{\sigma_m^3}{G_m^2(T,X)} \quad (3)$$

where

σ_m: the molar solid/liquid interfacial energy

G_m: Gibbs energy of the liquid-crystal transformation

N_a: Avogadro's number

Following Turnbull's approach [Turnbull 1950] $\sigma_m = 0.43 \Delta_{fus}H$ was used where $\Delta_{fus}H$ is the molar heat of fusion. The transformation energy was calculated with the following equation.

$$G_m(T,X) = G^L(T,X_L) - G^S(T,X_S) + \frac{dG^L(T,X_L)}{dX}(X_S - X_L) \quad (4)$$

where X is the mole fraction of Th. The terms in equation (4) are defined by illustration in the 700°C G-X diagram of the system (Figure 6) with solid phase being Fe_3Th_7,

$T = 700°C$ and $X = X_L = 0.6$.

The growth rate of a nucleus is

$$U_c = \frac{f\, D_g}{a_0} \left(1-\exp(-G_m(T,X)/RT)\right) \qquad (5)$$

where

D_g: the diffusion coefficient of liquid controlling growth

f: the fraction of atomic sites at the liquid/crystal interface (0 - 1)

On the basis of the Stokes - Einstein equation, D_g and D_n were assumed as

$$D_n = D_g = D = kT/3\eta a_0 \qquad (6)$$

where η is the viscosity of undercooled liquid and D is the bulk diffusion coefficient of liquid. Since the experimental viscosity of the liquid phase was not available between the melting temperature and the glass transition temperature, the free volume model suggested by Ramachandrarao et al. [1977] was used. The viscosity with the model is

$$\eta = \eta_0 \exp(1/f_v) \quad (7)$$

$$f_v = a_1 \exp(-E_h/RT) \quad (8)$$

$$E_h = 57.865\ T_g - 5857.6\ (J/mol) \quad (9)$$

where f_v is the free volume fraction, E_h is the energy of vacancy formation and η_0 and a_1 are constants. Equation (9) was derived empirically by Ramachandrarao et al. η_0 and a_1 were evaluated by the condition that

$$\eta = 10^{12}\ N/msec \text{ and } f_v = 0.03 \text{ when } T = T_g \quad (10)$$

which is considered to be a characteristic of glass transition materials. In equation (10) T_g is the glass transition temperature.

T_g values as a function of composition were not available for the Fe-Th system. However for many glasses glass transition temperature vs. melting temperature (T_g/T_m) which is called the reduced glass transition temperature is near constant and T_g is very similar to crystallization temperature (T_x) [Reeve et al. 1982] though T_g is less sensitive to the cooling rate ($\dot{T}$) than T_x is [Massalski et al. 1983]. It was reported that T_g/T_m was about 0.25 for pure metals and 0.45 to 0.65 for easy glass forming alloys [Davies 1976]. For the calculation T_g/T_m values were assumed to be 0.25 at X= 0 and 1 increasing to

0.5 at X= 0.5, so that

$$T_g/T_m = 0.25 + 0.5X \quad \text{when } 0< X <0.5$$
$$= 0.25 + 0.5(1-X) \quad \text{when } 0.5< X < 1 \qquad (11)$$

T_g and T_m values with composition are shown in Figure 8. From equations (1),(2),(5) and (7), t is given as

$$t = \frac{9.3}{kT} \left(\frac{a_0^9 x_f}{f^3 N_v}\right) \frac{\exp(\Delta_M G^*(T,X)/kT)}{(1-\exp(G_m/RT))^3}^{1/4} \qquad (12)$$

With equation (12), TTT curves were calculated for all solid phases. The critical cooling rate (R_c) with composition change was derived by

$$R_c = \frac{T_m - T_n}{t_n} \qquad (13)$$

where T_n = the nose temperature

t_n = the time at the nose

RESULTS AND DISCUSSION

T_0 curves determination

For the calculation of T_0 curves, it was necessary to evaluate the Gibbs energy of undercooled liquid over the range from glass transition temperature (T_g) to the melting temperature (T_m) [Sommer 1985]. Because of the lack of heat capacity (C_p) data, Δc_p^{l-g} was assumed to be zero. Then, with the previously evaluated Gibbs energy functions for the solution phases, T_0 curves for fcc, bcc1 and bcc2 were calculated and are shown in Figure 7. The resulting T_0 curves, which imply a wide glass forming region in the system, fall quite rapidly so that partitionless crystallization of the terminal solid solutions is indicated to be very limited [Boettinger 1982a, 1982b]. Near room temperature (27°C), T_0 occurs at 20.5 at.% Th and 79.2 at.% Th for bcc1 phase, 18.4 at.% Th and 79.8 at.% Th for bcc2 and 20.9 at.% Th and 74.3 at.% Th for fcc phase.

TTT curves determination

For the calculation of TTT curves, N_v, a_0, X_f and f, which are, respectively, 5E28 atoms/m^3, 3.6E-10 m, 1E-6 and 0.1, were used in equation (12). Typical TTT curves for the solid phases are shown in Figures 9-19 from 0 to 100 at.% Th with an interval of 10 at.% Th. Values from the

TTT curves for T_n and t_n were used to calculate the R_c's. Characteristic quantities associated with the TTT curves of all solid phases in the system are given in Tables 14 through 21. With data from Tables 14 - 21, critical cooling rates were calculated and are shown in Figure 20. It may be noted that the critical cooling rate for each phase is maximum at its own stoichiometric composition because the maximum driving force toward crystallization exists at stoichiometry. Fe_7Th_2 and Fe_5Th phases are less stable than the other phases so their critical cooling rate curves are less than those of other phases. The critical cooling rate curves of the terminal solid solution phases (bcc1(α), bcc2(δ) and fcc) are quite similar to the T_0 curves. Table 22 shows data for the phases in which glass formation would be most difficult. With a cooling rate of 1E 6 (K/sec), the possible glass forming region is 45 - 52 at.% Th which is consistent with glass formation that has been observed at 50 at.% Th by the melt spinning process ($\dot{T}$ = 1E 6 K/sec) [Drehman, private communication 1985]. The glass forming region determined from T_0 curves is compared with that from TTT curves in Figure 21. Figure 21 shows that at high cooling rates ($\dot{T}$ > 1E 9 K/sec), glass formation is competing with composition-invariant phase crystallization [Massalski et al. 1983]. However glass can be formed outside the glass forming regions that are

determined by T_0 curves if the cooling rates are above 1E10 K/sec [Lin et al. 1984]. It appears to be possible to form amorphous alloys throughout the whole composition range in this system if the cooling rates exceed 1E12 K/sec.

CONCLUSIONS

The glass forming ability of Fe-Th alloys was determined from TTT and T_0 curves with data for the thermodynamic and kinetic parameters being based upon input from the calculation of the equilibrium diagram. It has thus been demonstrated that the Gibbs energy functions describing the equilibrium phase diagram can be useful in deriving metastable as well as stable phase formation, and a complete assessment of the metastable equilibria should include consideration of equilibrium thermodynamic functions as well as kinetic factors.

Table 14. Characteristics of TTT Curves for bcc1 Phase

at.% Th	T_n(K)	t_n(sec)	R_c(K/sec)	$\log_{10}(R_c)$
0	965	0.39E-8	0.21E12	11.33
5	860	0.21E-7	0.41E11	10.60
10	770	0.19E-5	0.49E9	8.69
15	660	0.63	0.16E4	3.21
20 - 75	-	-	-	< -17
80	530	0.11E16	0.86E12	-12.06
85	690	0.31E-2	0.31E6	5.49
90	845	0.32E-6	0.30E10	9.48
95	990	0.82E-8	0.11E12	11.06
100	1125	0.13E-8	0.67E12	11.82

Table 15. Characteristics of TTT Curves for fcc Phase

at.% Th	T_n(K)	t_n(sec)	R_c(K/sec)	$\log_{10}(R_c)$
0	990	0.26E-8	0.31E12	11.49
5	870	0.14E-7	0.59E11	10.76
10	780	0.12E-5	0.73E9	8.66
15	665	0.31	0.32E4	3.51
20 - 70	-	-	-	< -17
75	520	0.36E20	0.25E-16	-16.58
80	635	0.40E1	0.22E3	2.35
85	755	0.32E-4	0.28E8	7.45
90	870	0.24E-6	0.39E10	9.59
95	970	0.16E-7	0.58E11	10.77
100	1060	0.33E-8	0.28E12	11.45

Table 16. Characteristics of TTT Curves for bcc2 Phase

at.% Th	T_n(K)	t_n(sec)	R_c(K/sec)	$\log_{10}(R_c)$
0	1000	0.22E-8	0.36E12	11.56
5	870	0.12E-7	0.64E11	10.81
10	760	0.22E-5	0.43E9	8.63
15	620	0.29E3	0.37E1	0.57
20 - 75	-	-	-	< -17
80	510	0.84E20	0.12E-16	-16.91
85	685	0.55E-2	0.18E6	5.25
90	845	0.31E-6	0.31E10	9.49
95	990	0.79E-8	0.11E12	11.07
100	1125	0.13E-8	0.67E12	11.82

Table 17. Characteristics of TTT Curves for Fe_3Th_7 Phase

at.% Th	T_n(K)	t_n(sec)	R_c(K/sec)	$\log_{10}(R_c)$
0 -30	-	-	-	<-17
35	635	0.13E11	0.59E7	-7.22
40	695	0.66E4	0.10	-0.98
45	750	0.15E1	0.35E3	2.55
50	785	0.10E-1	0.44E5	4.64
55	780	0.21E-4	0.17E8	7.23
60	795	0.48E-5	0.81E8	7.91
65	795	0.17E-5	0.25E9	8.39
70	805	0.18E-5	0.27E9	8.44
75	815	0.39E-5	0.16E9	8.21
80	795	0.72E-5	0.10E9	8.02
85	770	0.35E-4	0.25E8	7.40
90	730	0.75E-3	0.14E7	6.16
95	660	0.34	0.37E4	3.57
100	-	-	-	< -17

Table 18. Characteristics of TTT Curves for Fe_3Th Phase

at.% Th	T_n(K)	t_n(sec)	R_c(K/sec)	$\log_{10}(R_c)$
0	475	0.19E14	0.66E-10	-10.17
5	730	0.12E-4	0.80E8	7.90
10	805	0.87E-5	0.10E9	8.02
15	850	0.85E-5	0.10E9	8.00
20	870	0.81E-5	0.92E8	7.96
25	870	0.66E-5	0.97E8	7.98
30	880	0.13E-4	0.42E8	7.63
35	885	0.41E-4	0.13E8	7.12
40	880	0.13E-3	0.37E7	6.57
45	860	0.45E-3	0.99E6	5.99
50	835	0.19E-2	0.20E6	5.31
55	765	0.46E-3	0.82E6	5.91
60	725	0.28E-2	0.16E6	5.20
65	685	0.30E-1	0.17E5	4.25
70	805	0.86E1	0.77E2	1.88
75	610	0.55E6	0.15E-2	-2.81
80	560	0.81E13	0.12E-9	-9.91
85 - 100	-	-	-	<-17

Table 19. Characteristics of TTT Curves for Fe_7Th_2 Phase

at.% Th	T_n(K)	t_n(sec)	R_c(K/sec)	$\log_{10}(R_c)$
0	515	0.29E8	0.44E-4	-4.35
5	715	0.96E-4	0.10E8	7.00
10	775	0.13E-3	0.71E7	6.85
15	810	0.20E-3	0.43E7	6.63
20	825	0.26E-3	0.29E7	6.47
25	820	0.25E-3	0.27E7	6.44
30	830	0.76E-3	0.84E6	5.92
35	835	0.36E-2	0.16E6	5.22
40	830	0.17E-1	0.32E5	4.51
45	810	0.80E-1	0.62E4	3.79
50	790	0.44	0.99E3	2.99
55	725	0.44E-1	0.95E4	3.98
60	695	0.30	0.16E4	3.21
65	655	0.31E1	0.18E3	2.26
70	630	0.11E4	0.60	-0.21
75	605	0.69E8	0.12E-4	-4.90
80	560	0.11E15	0.84E-11	-11.07
85 - 100	-	-	-	<-17

Table 20. Characteristics of TTT Curves for Fe_5Th Phase

at.% Th	T_n(K)	t_n(sec)	R_c(K/sec)	$\log_{10}(R_c)$
0	570	0.13E2	0.89E2	1.95
5	810	0.52E-6	0.16E10	9.22
10	870	0.64E-6	0.13E10	9.12
15	900	0.95E-6	0.83E9	8.92
20	910	0.14E-5	0.50E9	8.70
25	900	0.18E-5	0.34E9	8.53
30	895	0.53E-5	0.10E9	8.03
35	890	0.25E-4	0.21E8	7.33
40	870	0.14E-3	0.34E7	6.53
45	840	0.11E-2	0.40E6	5.60
50	805	0.15E-1	0.27E5	4.44
55	725	0.62E-2	0.67E5	4.83
60	680	0.21	0.23E4	3.37
65	625	0.31E2	0.18E2	1.27
70	580	0.78E7	0.94E-4	-4.02
75 - 100	-	-	-	<-17

Table 21. Characteristics of TTT Curves for $Fe_{17}Th_2$ Phase

at.% Th	T_n(K)	t_n(sec)	R_c(K/sec)	$\log_{10}(R_c)$
0	665	0.89E-4	0.12E8	7.10
5	925	0.15E-7	0.50E11	10.70
10	980	0.20E-7	0.36E11	10.56
15	995	0.33E-7	0.20E11	10.31
20	990	0.60E-7	0.10E11	10.02
25	960	0.10E-6	0.51E10	9.71
30	940	0.40E-6	0.13E10	9.11
35	910	0.29E-5	0.18E9	8.25
40	870	0.40E-4	0.12E8	7.10
45	820	0.15E-2	0.32E6	5.51
50	760	0.36	0.12E4	3.11
55	660	0.71E1	0.27E3	2.44
60	590	0.18E6	0.31E-2	-2.49
65	515	0.63E16	0.11E-12	-12.95
70 - 100	-	-	-	<-17

Table 22. Critical Cooling Rate in the Th-Fe System

at.% Th	most competing phase	$\log_{10}$ (R_c)
0	bcc2	11.56
5	bcc2	10.81
10	$Fe_{17}Th_2$	10.56
15	$Fe_{17}Th_2$	10.31
20	$Fe_{17}Th_2$	10.02
25	$Fe_{17}Th_2$	9.71
30	$Fe_{17}Th_2$	9.11
35	$Fe_{17}Th_2$	8.25
40	$Fe_{17}Th_2$	7.10
45	Fe_3Th	5.99
50	Fe_3Th	5.31
55	Fe_3Th_7	7.23
60	Fe_3Th_7	7.91
65	Fe_3Th_7	8.39
70	Fe_3Th_7	8.44
75	Fe_3Th_7	8.21
80	Fe_3Th_7	8.02
85	fcc	7.45
90	fcc	9.59
95	bcc2	11.07
100	bcc1/bcc2	11.82

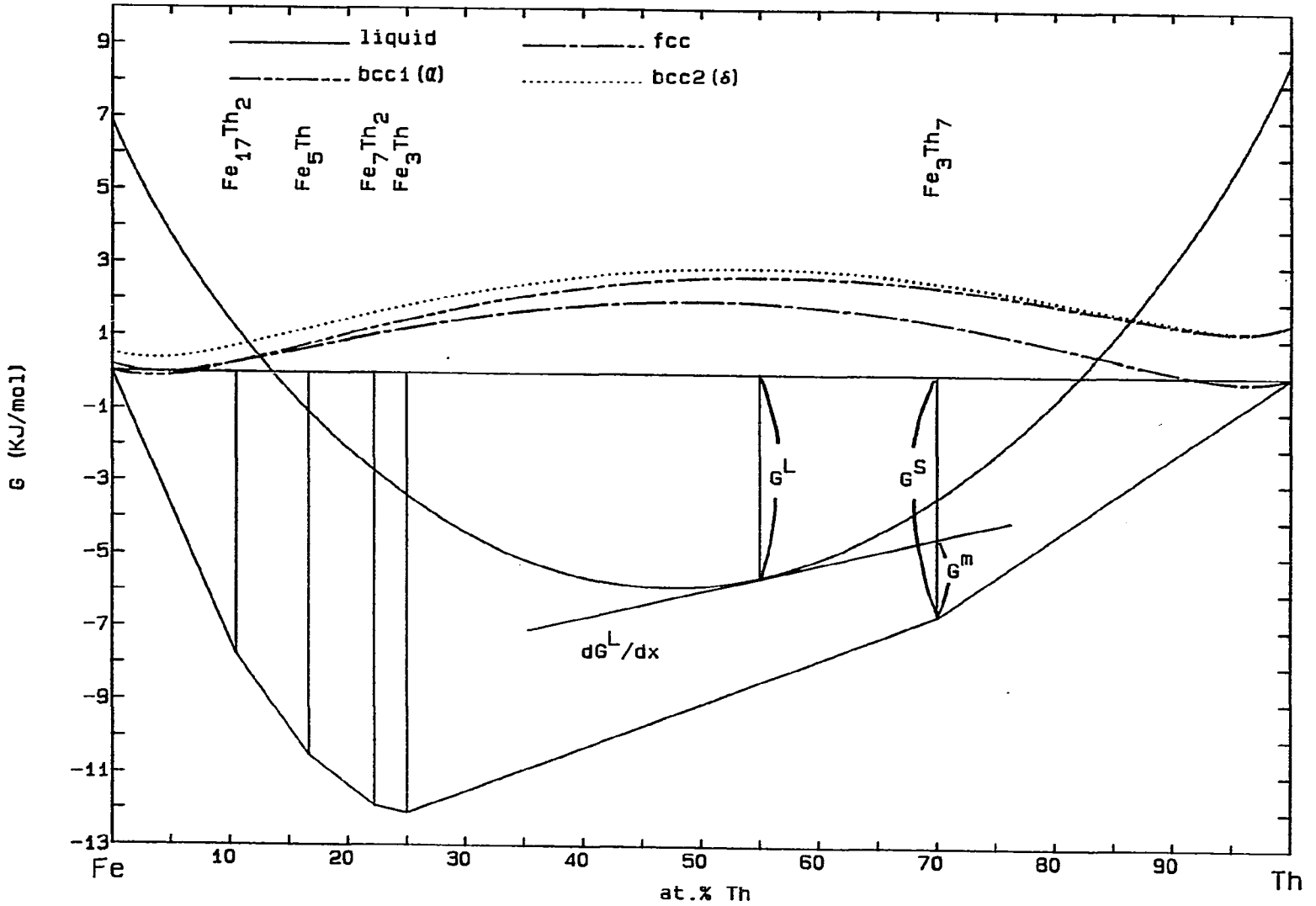

Fig. 6 The G-x diagram (700°C)

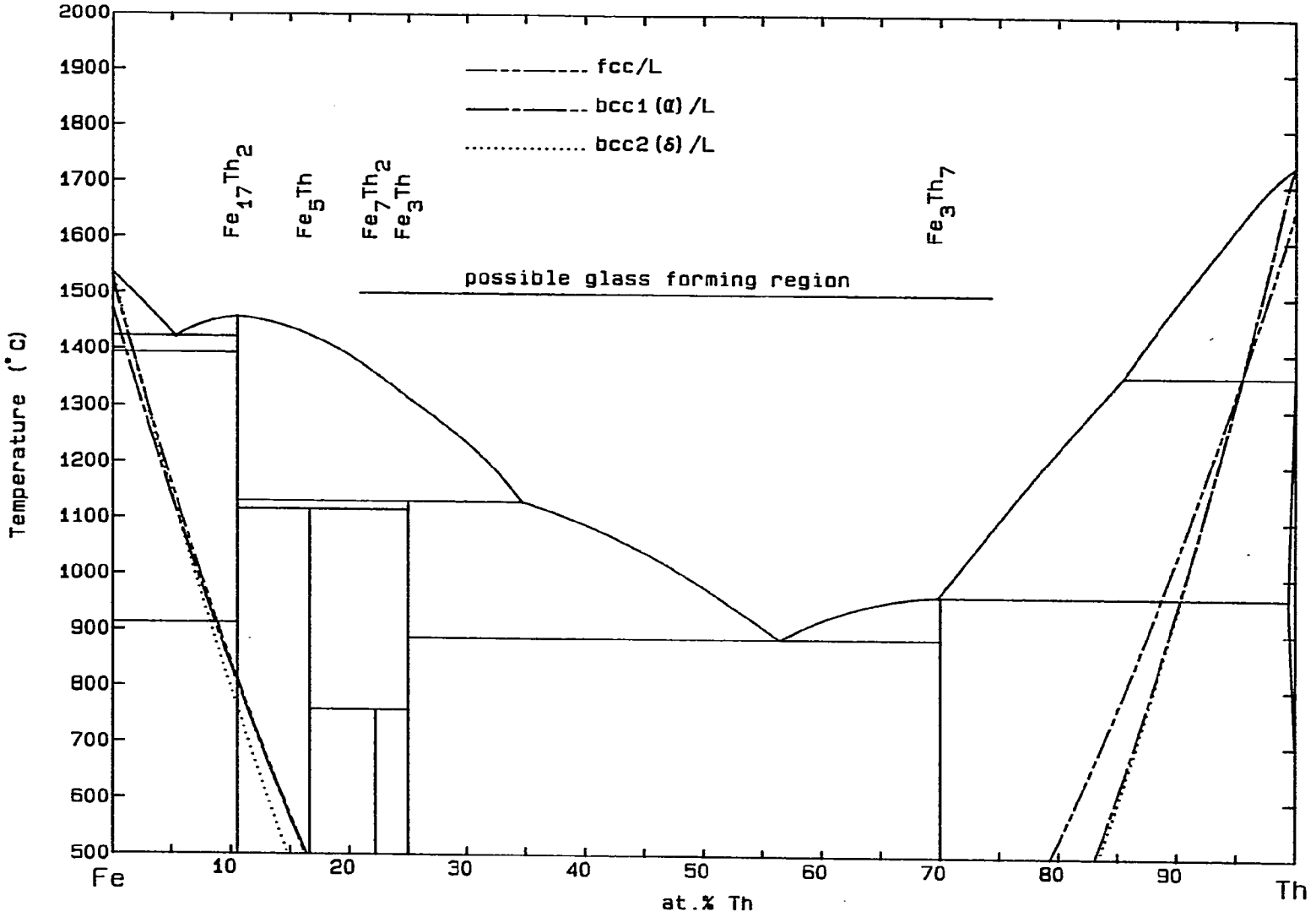

Fig. 7 The Fe-Th system (T_0 Curves)

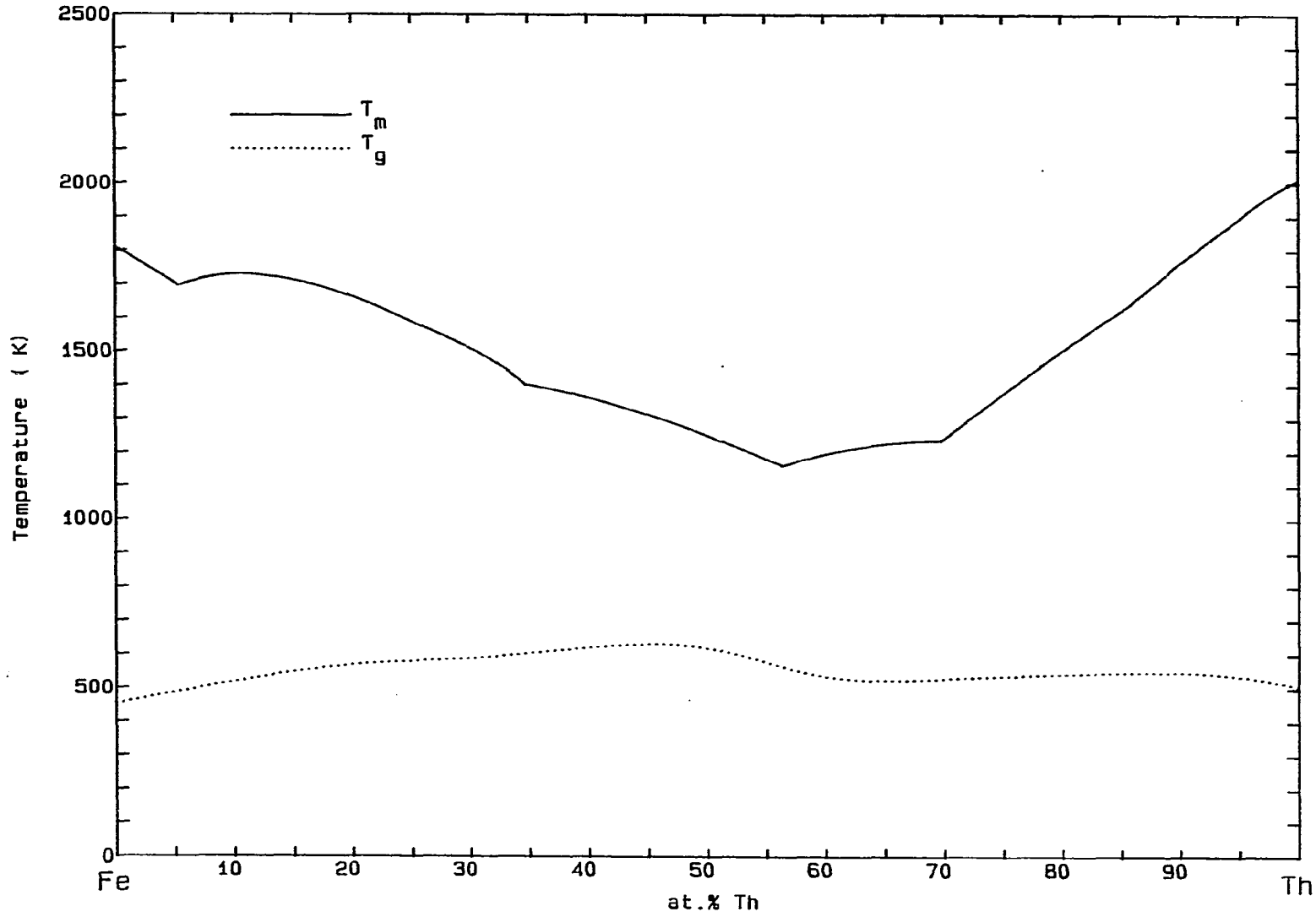

Fig. 8 T_m and T_g in the Fe-Th system

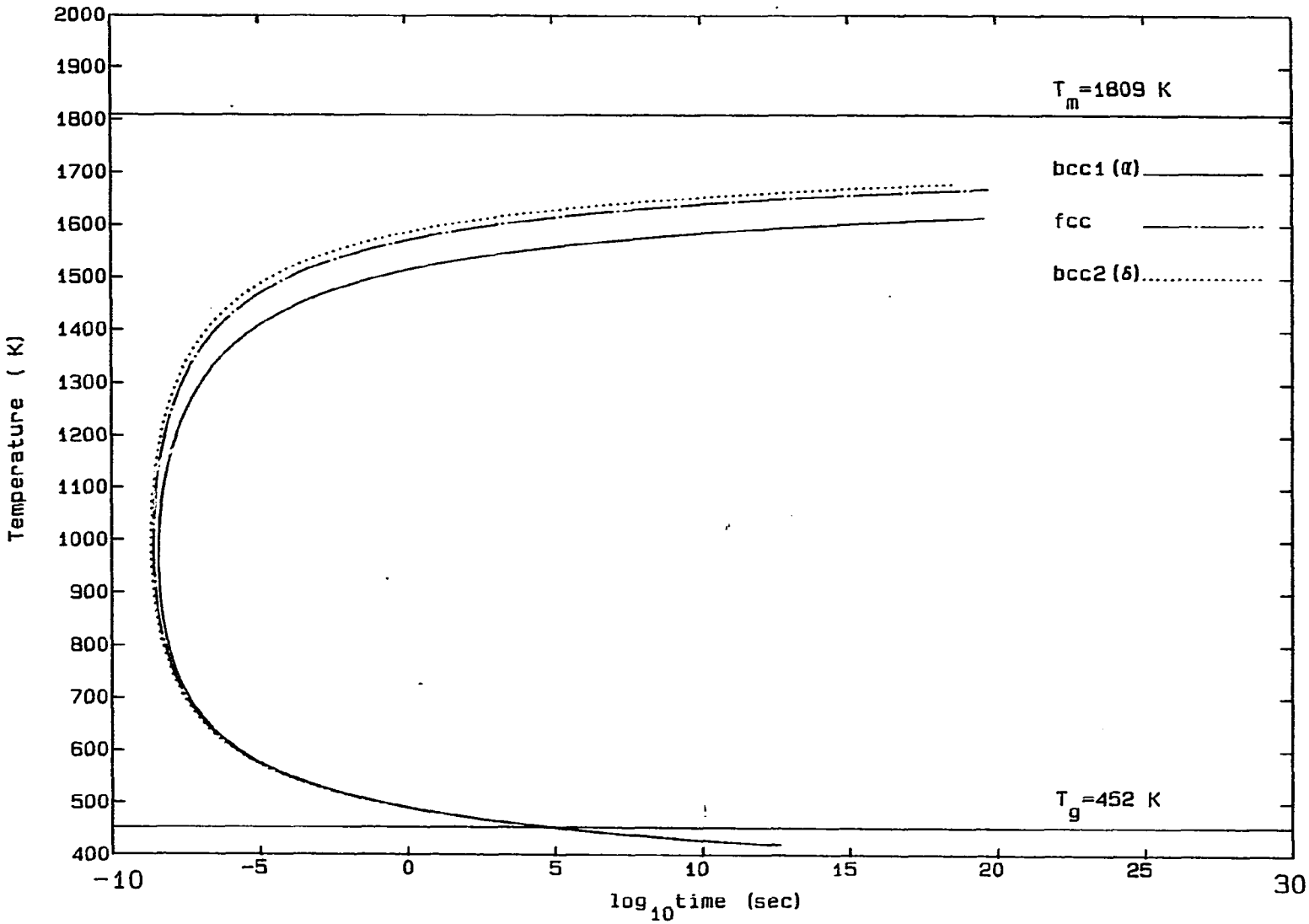

Fig. 9 TTT curves (0 at.% Th)

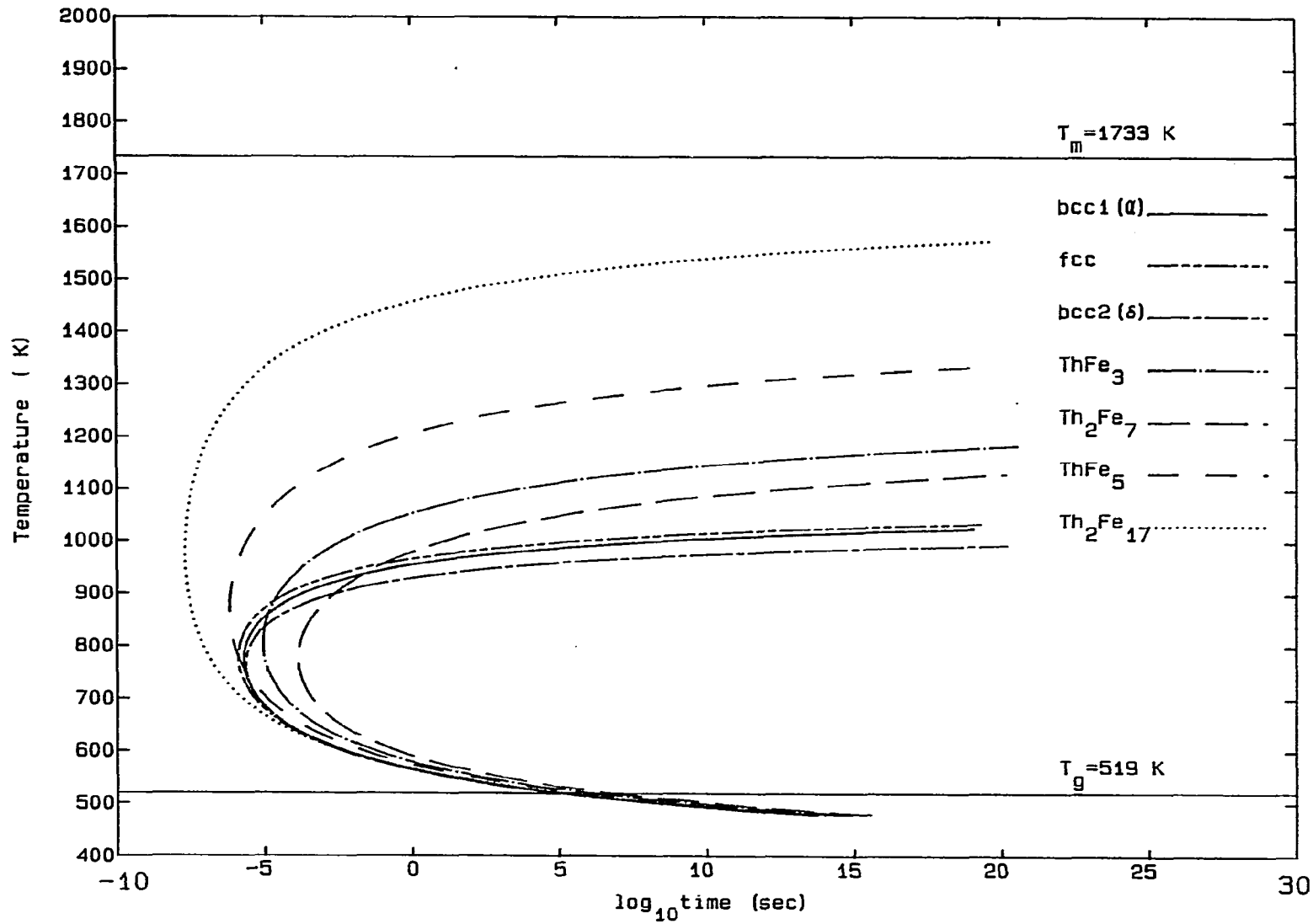

Fig. 10 TTT curves (10 at.% Th)

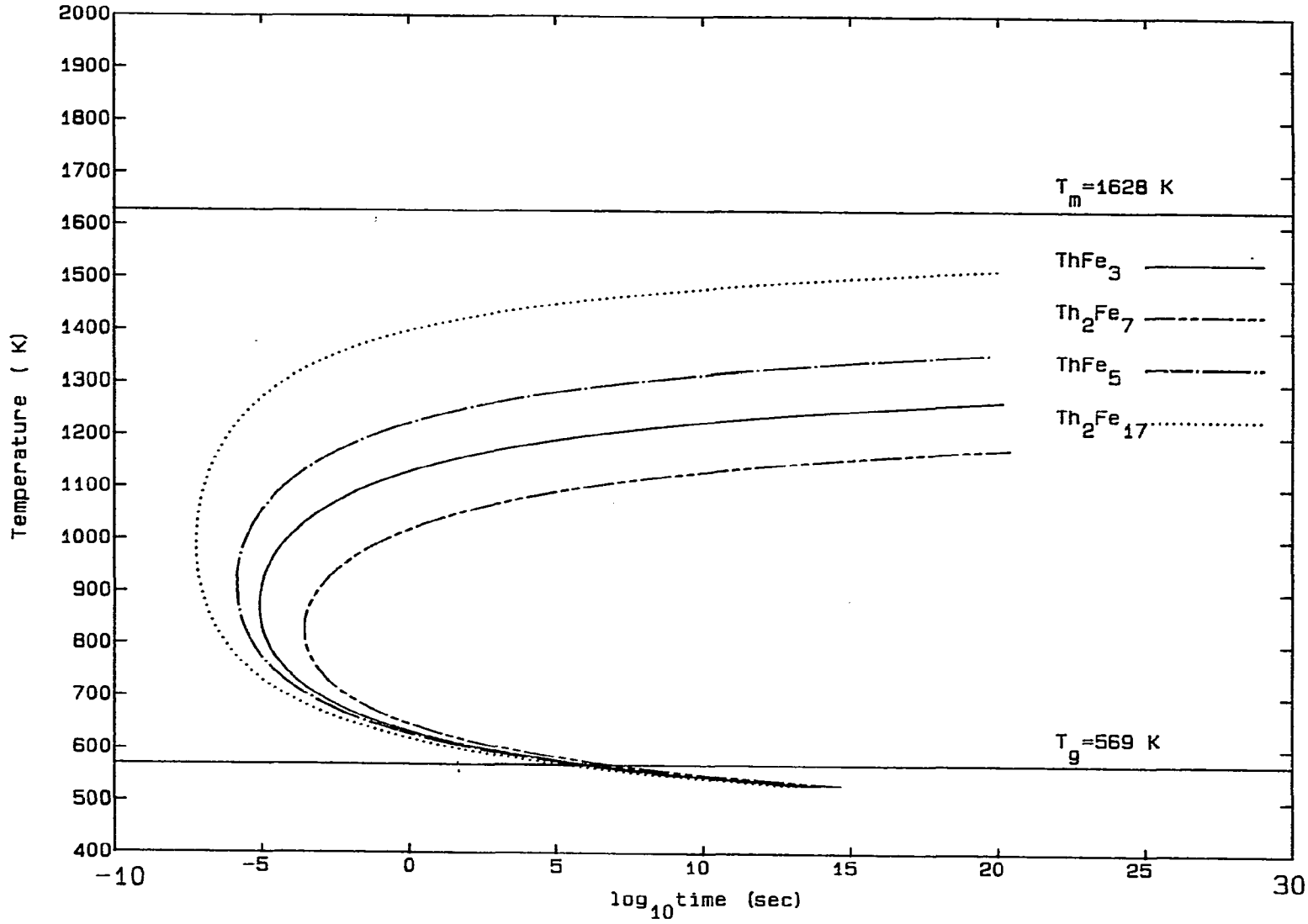

Fig. 11 TTT curves (20 at.% Th)

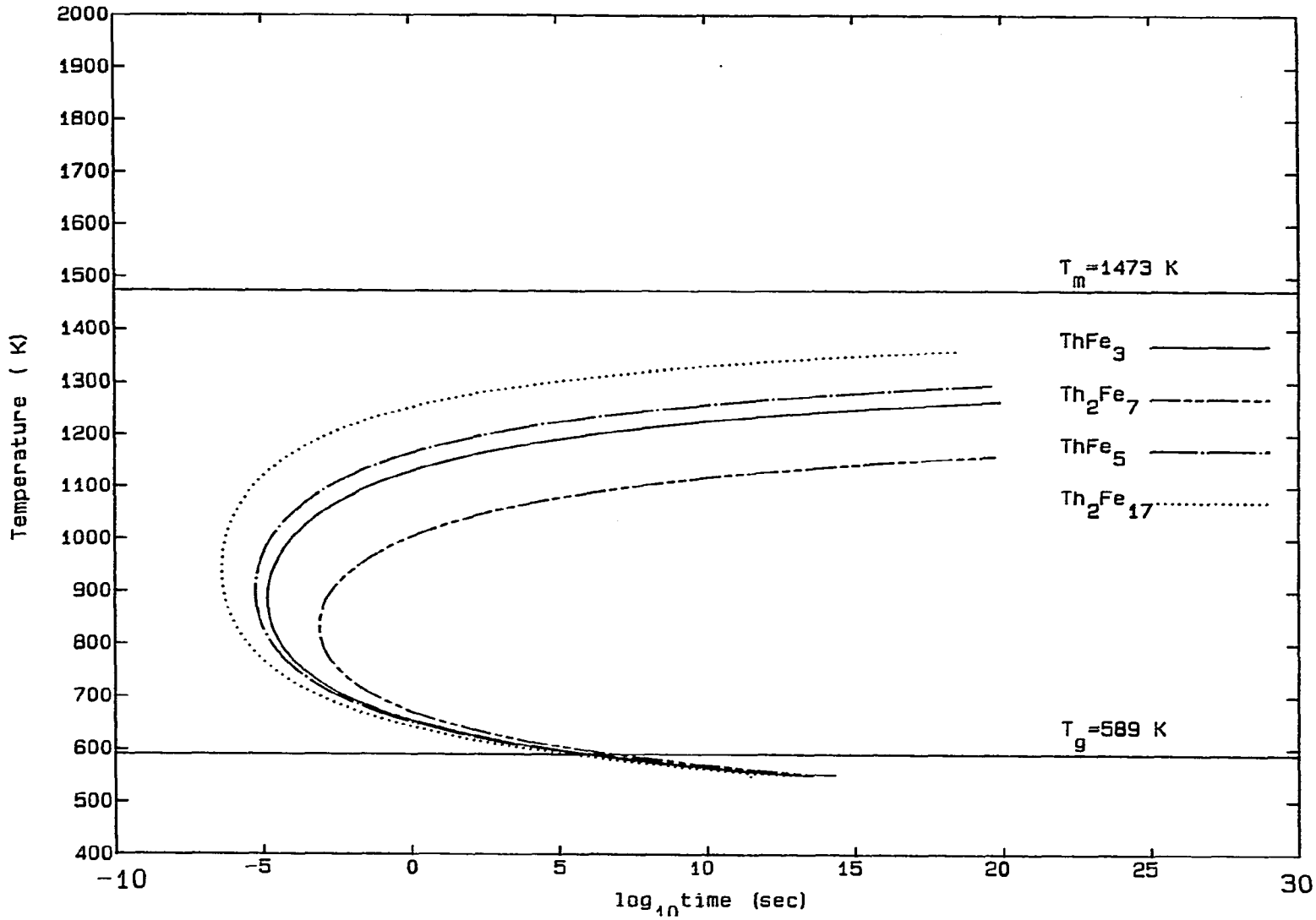

Fig. 12 TTT curves (30 at.% Th)

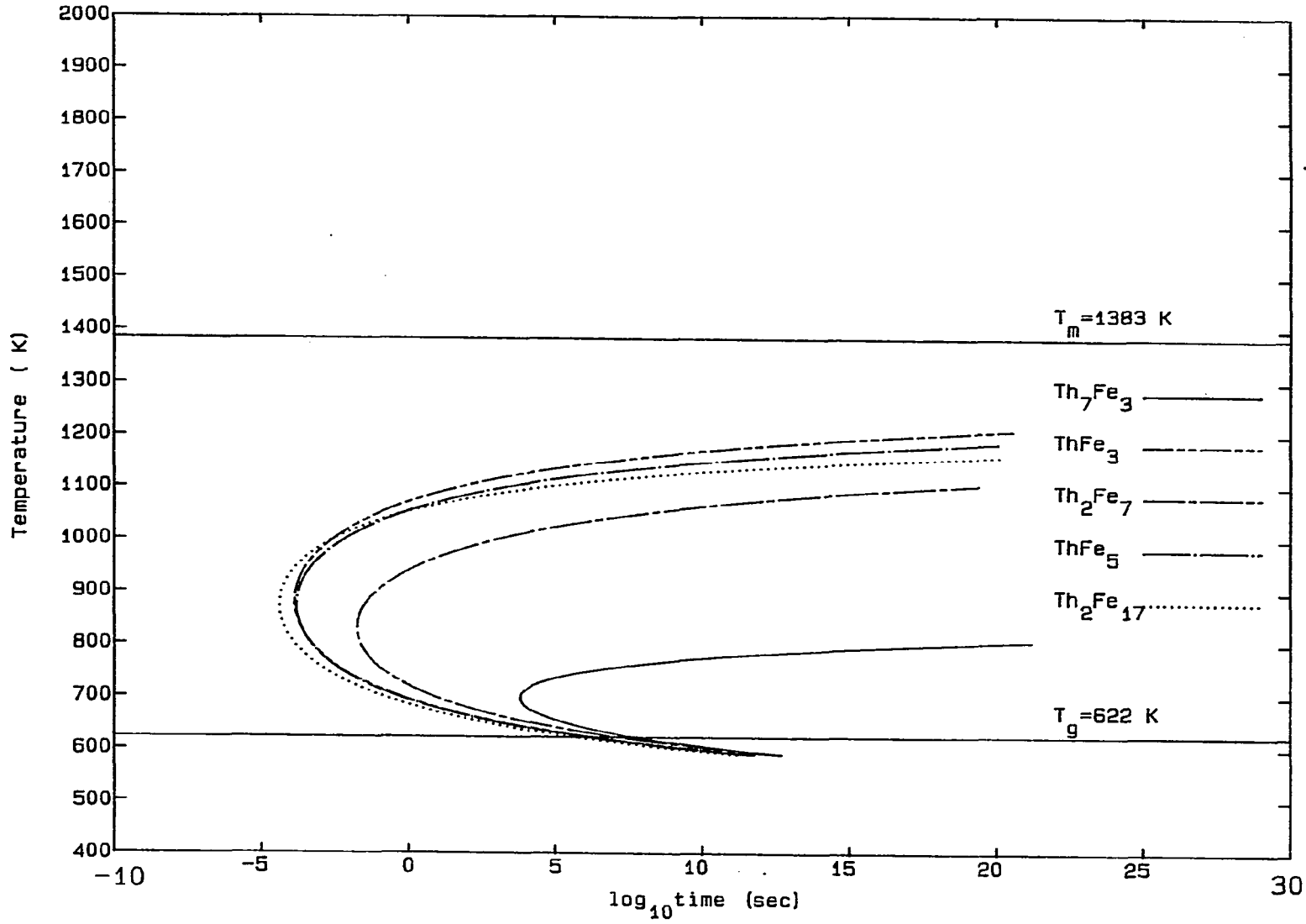

Fig. 13 TTT curves (40 at.% Th)

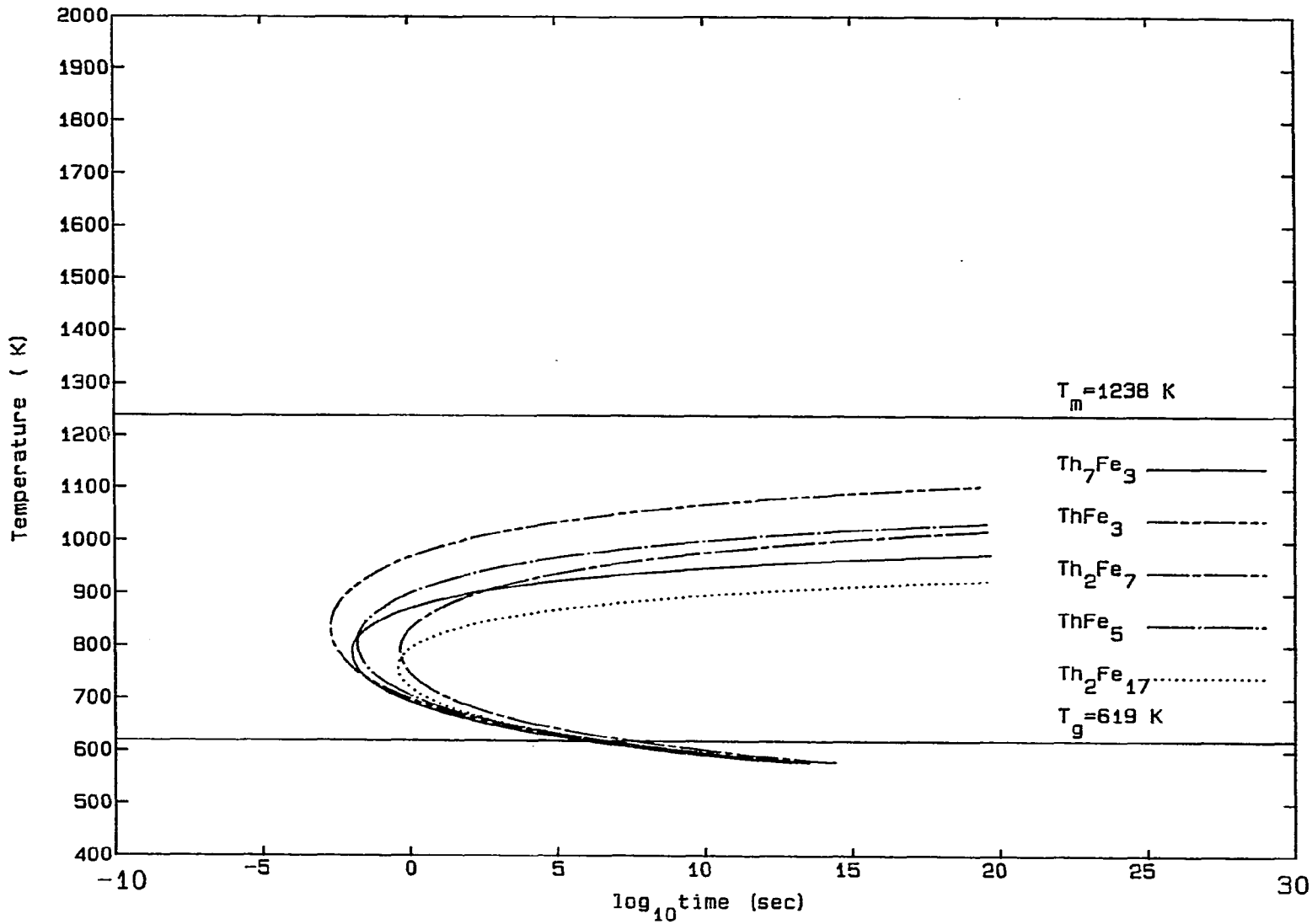

Fig. 14 TTT curves (50 at.% Th)

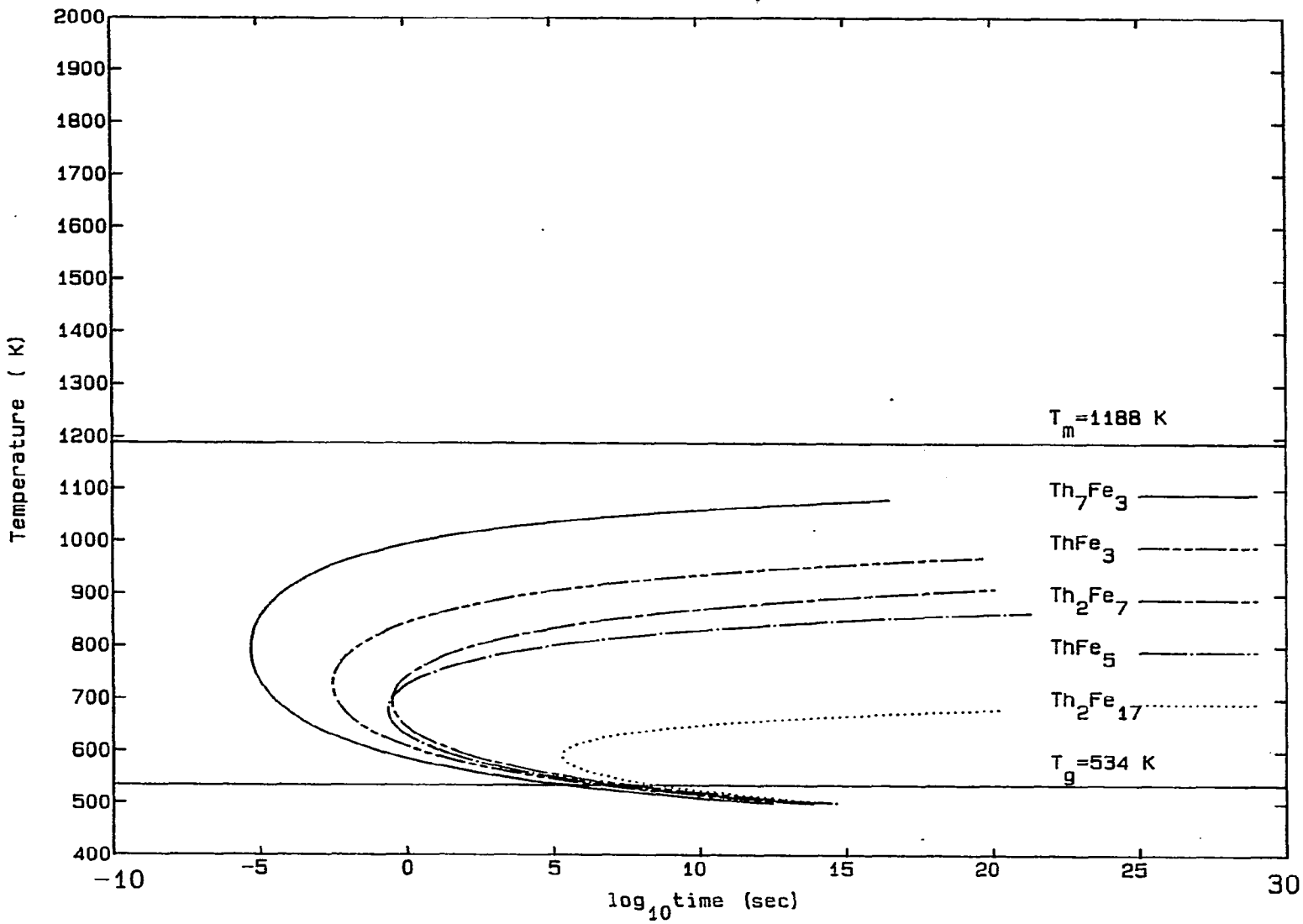

Fig. 15 TTT curves (60 at.% Th)

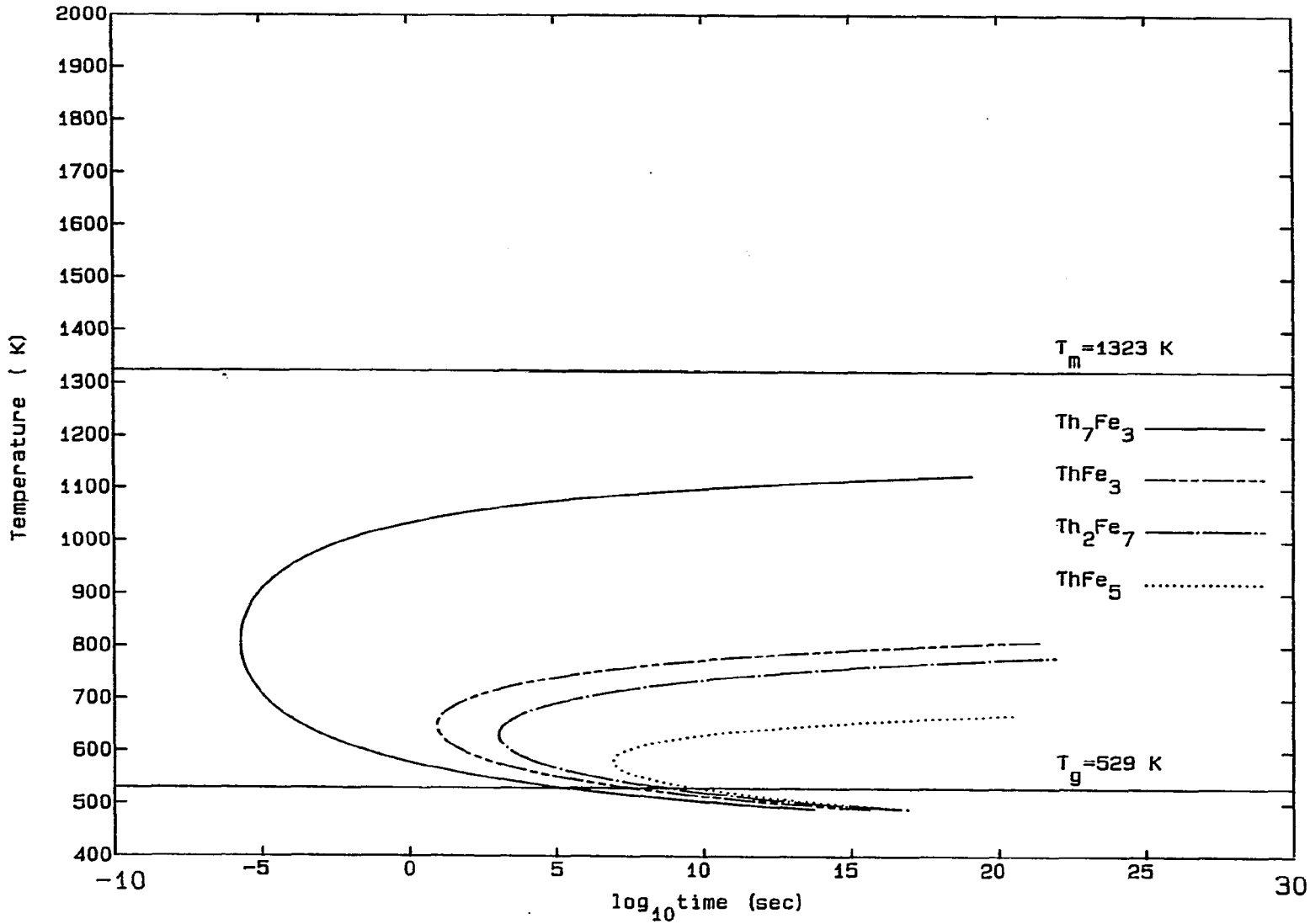

Fig. 16 TTT curves (70 at.% Th)

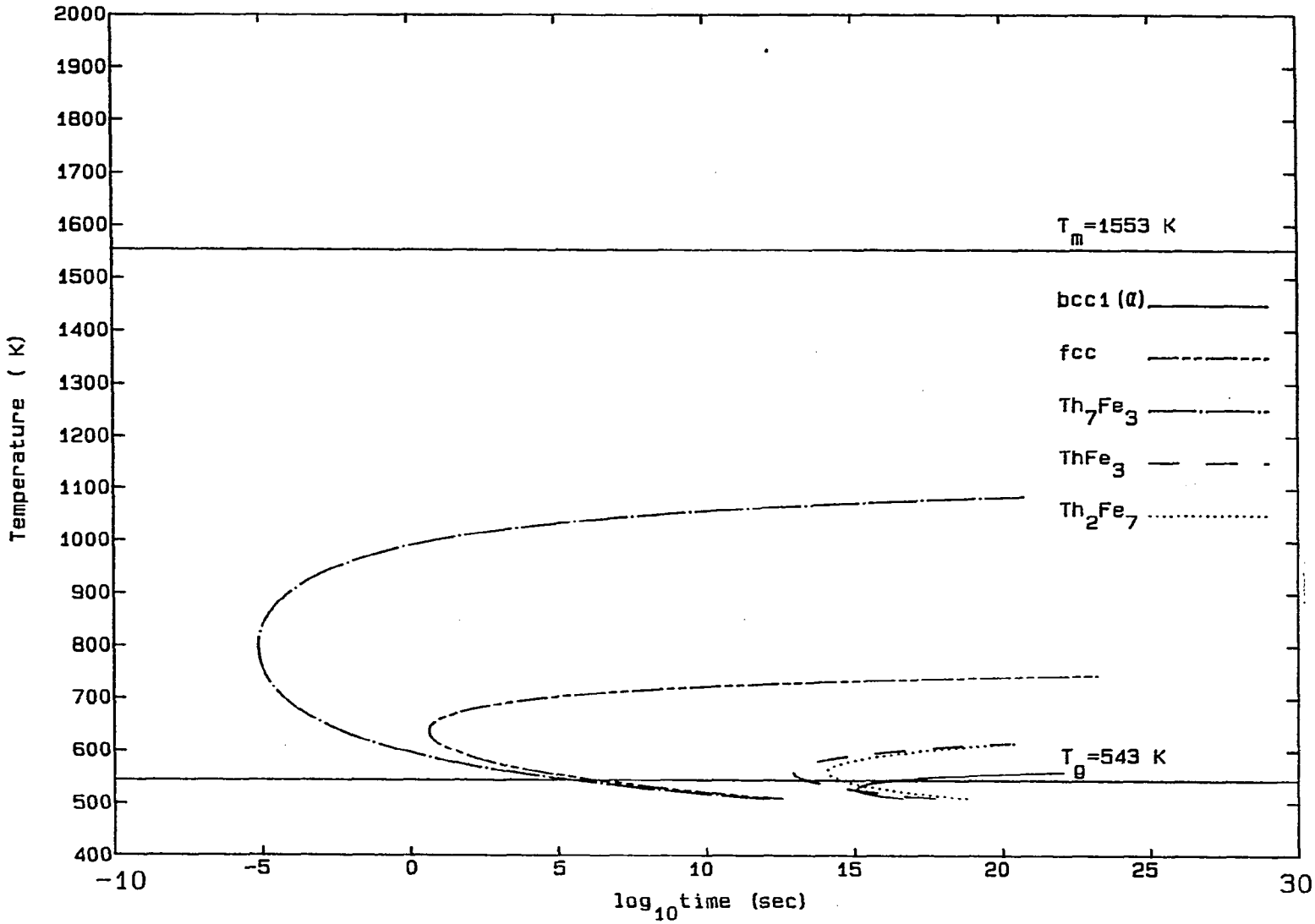

Fig. 17 TTT curves (80 at.% Th)

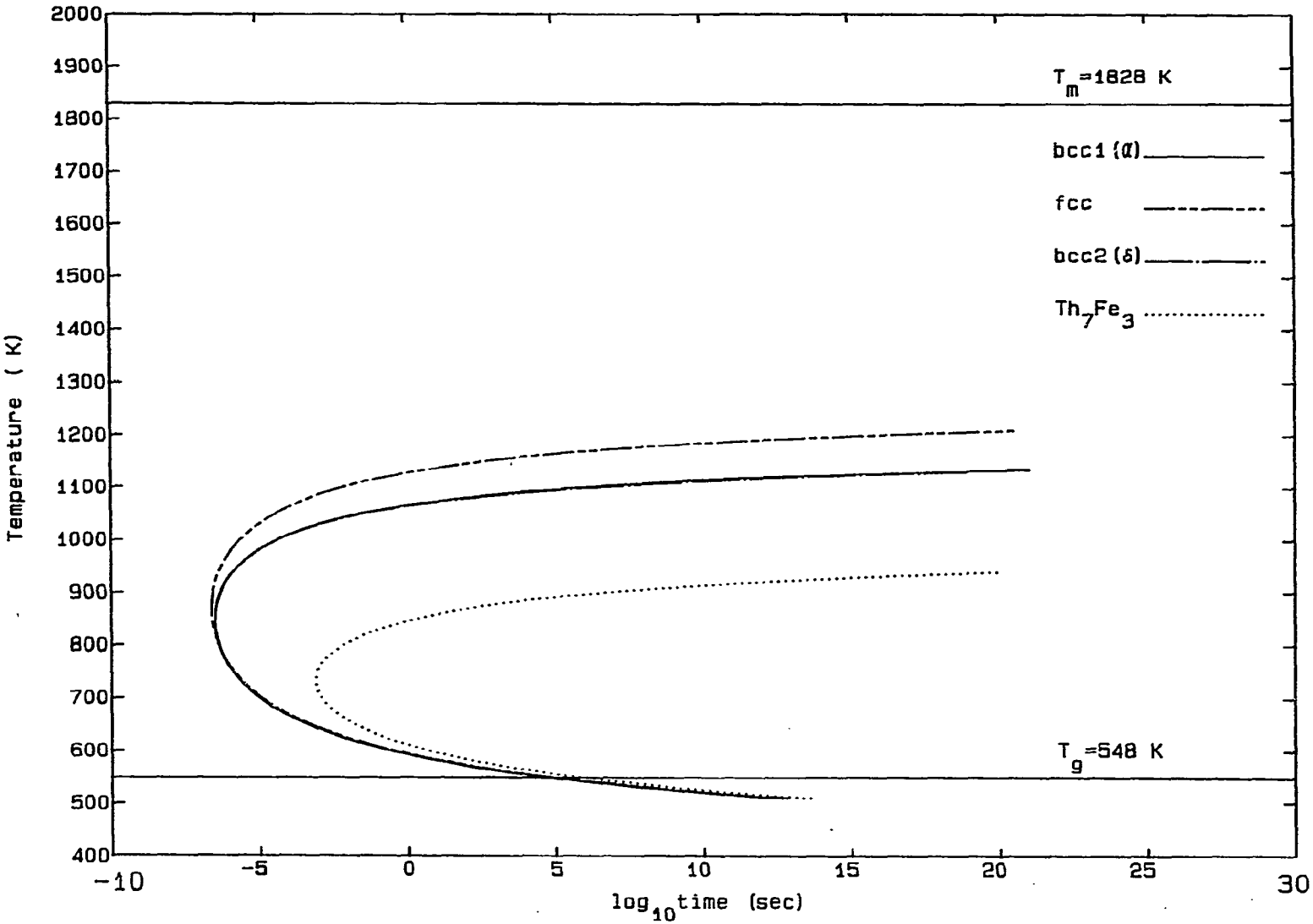

Fig. 18 TTT curves (90 at.% Th)

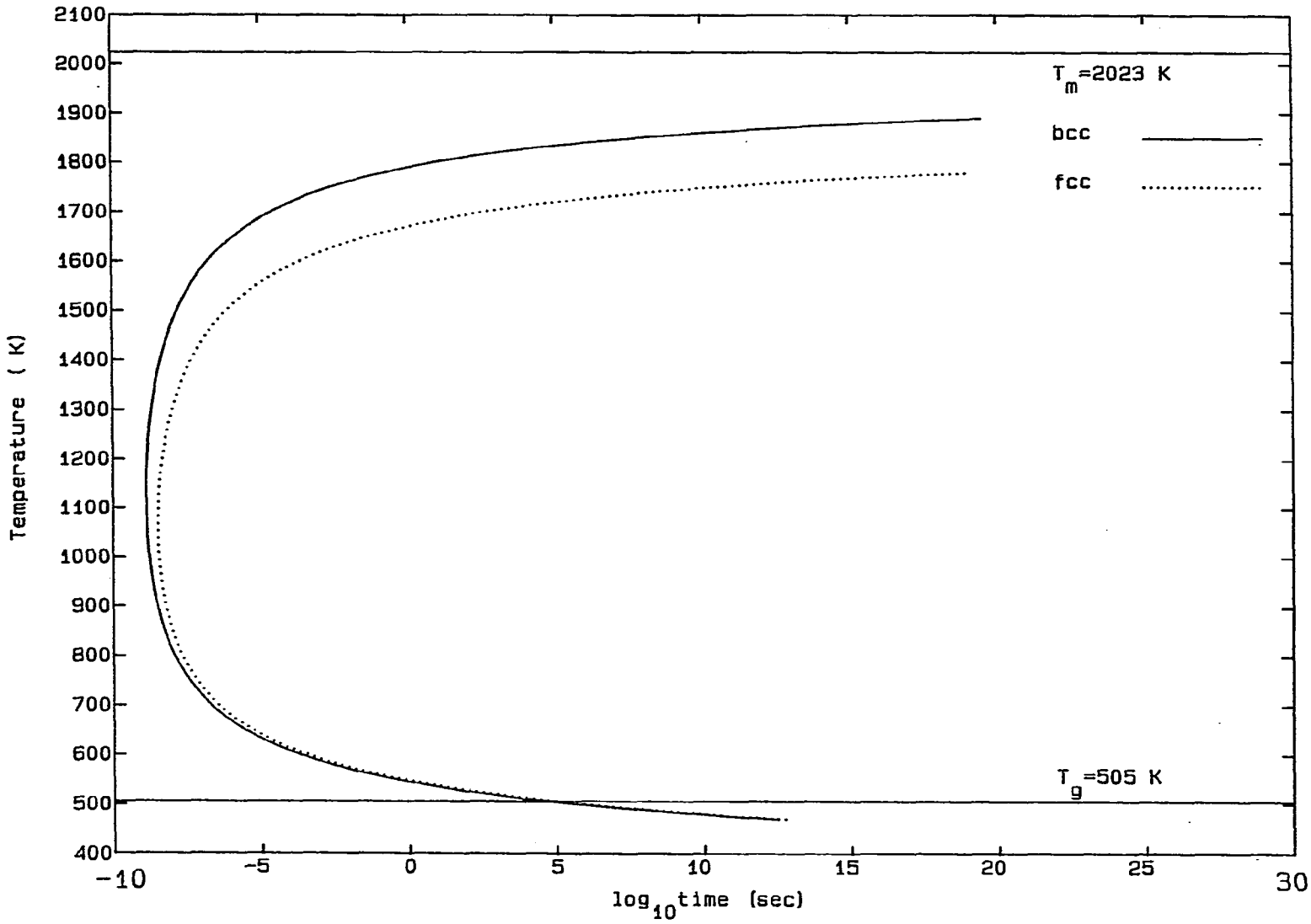

Fig. 19 TTT curves (100 at.% Th)

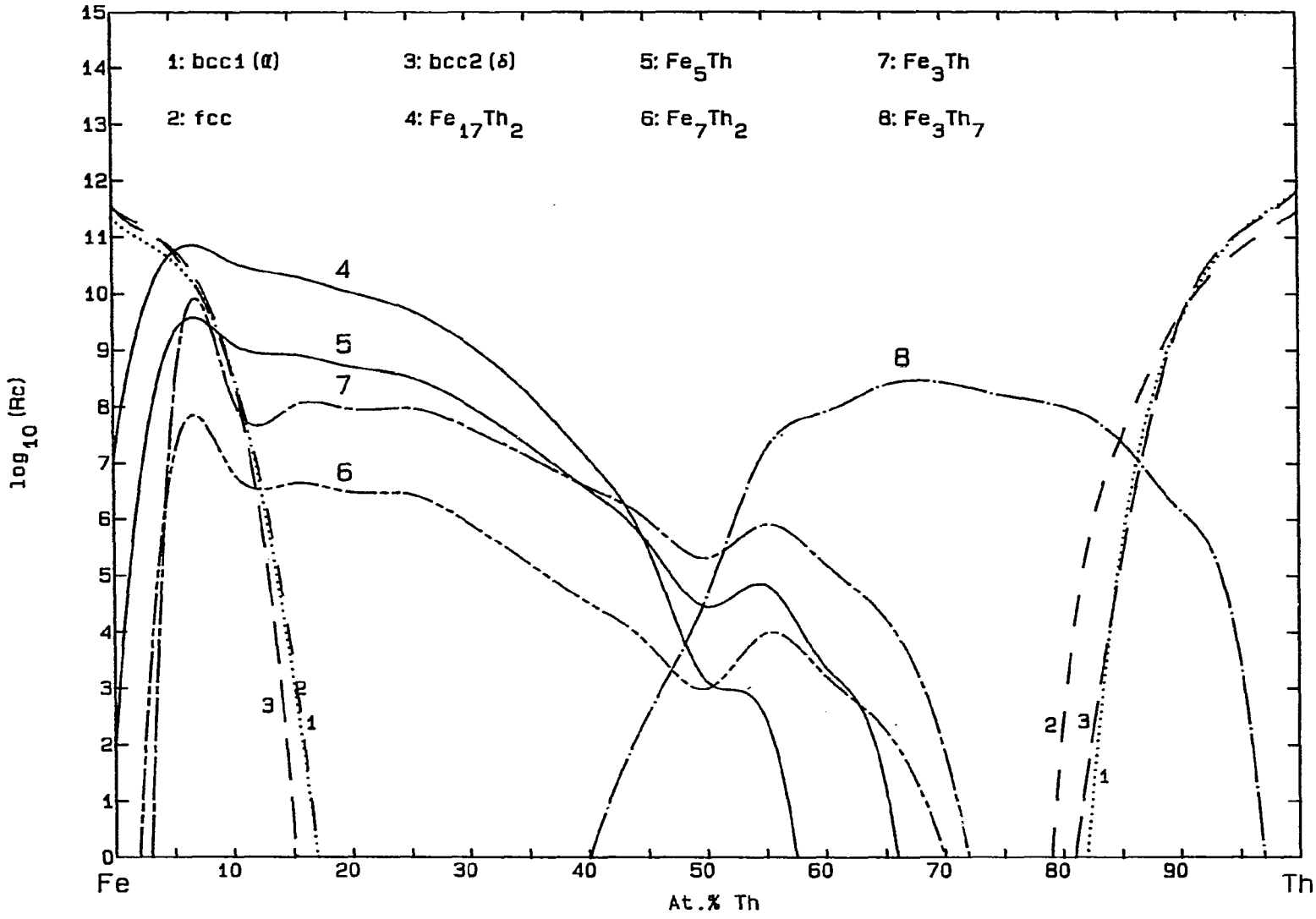

Fig. 20 Critical cooling rate (R_c) for solid phases

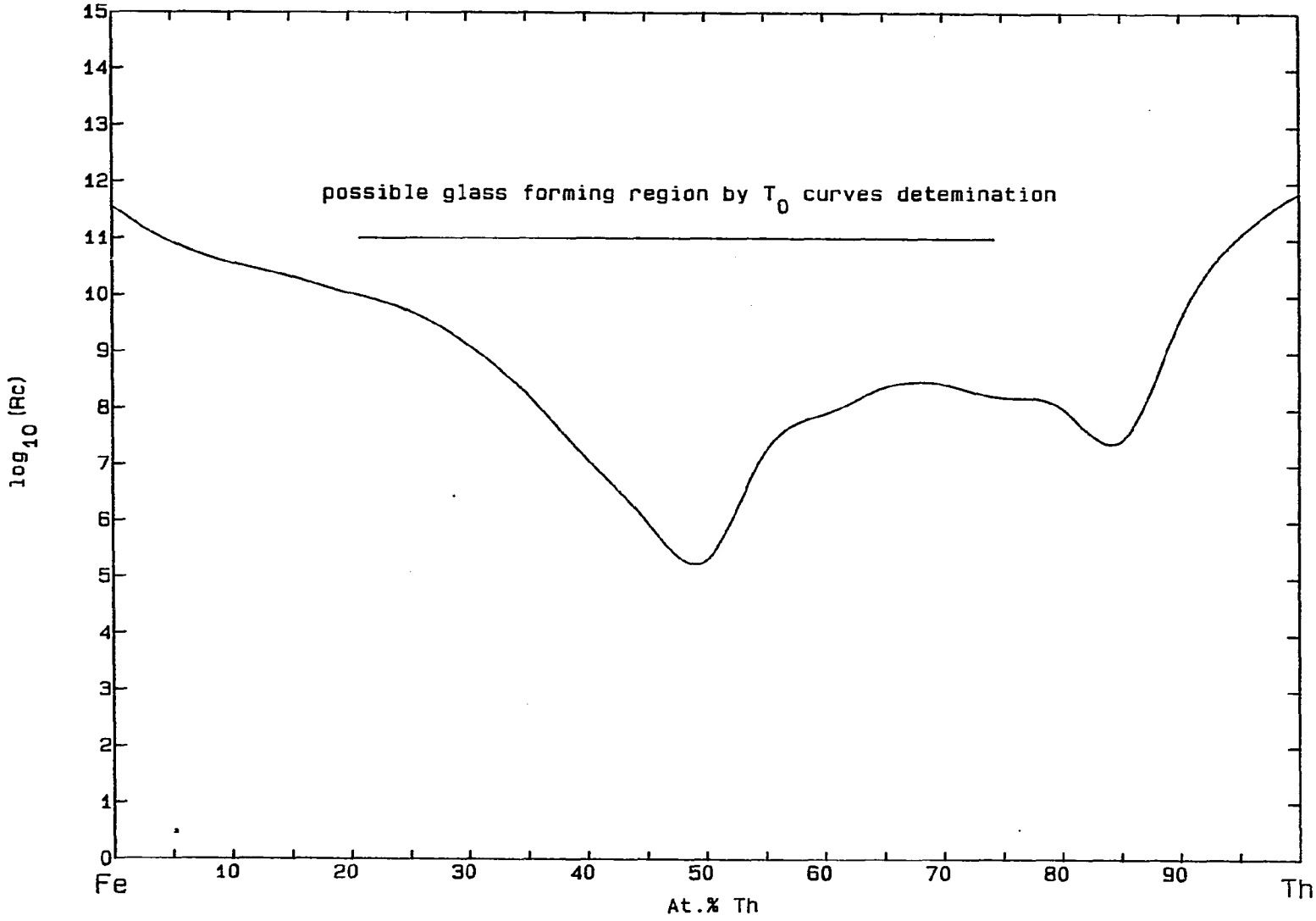

Fig. 21 Critical cooling rate (R_c) in the Fe-Th system

REFERENCES

Boettinger W. J., Rapidly Solidified Amorphous and Crystalline Alloys, B. H. Kear, B. C. Giessen and M. Cohen, eds. (Elsevier, New York, 1982a)

Boettinger W. J., Proc. 4th Int. conf. on Rapid Quenched Metals, (Sendai, Japan, 1982b)

Christian J. W., Theory of Phase Transformations in Metals and Alloys, (Pergamon, Oxford, 1965)

Davies H. A., Phys. Chem. Glasses, 17, 159 (1976)

Drehman A. J.; private communication (Former Ames Lab. Researcher)

Lin C. J., F. Spacen and D. Turnbull, J. Non-Cryst. Solids, 61/62, 767 (1984)

Massalski T. B., C. G. Woychik and J. L. Murray, Alloy Phase Diagrams, Mat. Soc. Symp. Proc. Vol. 19 (Elsevier Science Pub. Co. Inc., New York, 1983)

Perepezko J. H., Alloy Phase Diagrams, Mat. Soc. Symp. Proc. Vol. 19 (Elsevier Science Pub. Co. Inc., New York, 1983)

Polk D. E. and B. C. Giessen, Metallic Glasses, (ASM, Metals Park, Ohio, 1978)

Ramachandrarao P., B. Cantor and R. W. Chan, J. Mater. Sci., 12, 2488 (1977)

Reeve J., H. A. Davies and I. W. Donald, Proc. 4th Int. Conf. on Rapid Quenched Metals, (Sendai, Japan, 1982)

Sommer F., Proc. 5th Int. Conf. on Rapidly Quenched Metals, S. Steeb and H. Warlimont eds. (Elsevier Science Pub. Co. Inc., New York, 1985)

Turnbull D., J. Appl. Phys. 21, 1022 (1950)

OVERALL SUMMARY

It was not the purpose of this study to reevaluate the phase diagram, but rather to generate internally consistent thermodynamics functions for each phase. From the phase diagram information, mostly invariant reactions, experimental data and a theoretical model, such thermodynamic descriptions for the phases were obtained with input information. First, all available thermodynamic data were assembled and a model which satisfactorily fits the experimental data was developed. Since any regression creates a best fit to all data, parameters were reevaluated such that they predicted certain critical phase diagram areas exactly along with representing the thermodynamic property. The second and third step in this study was set up in a way that each step optimized the parameters such that the difference between evaluated phase diagram and calculated one is approximately zero.

This analysis indicates that thermodynamic data alone can not be relied upon to predict the phase boundary behavior. Both thermodynamic data and phase diagram data should be used.

The glass forming ability of Fe-Th alloys was determined from TTT and T_0 curves with data for the thermodynamic and kinetic parameters being based upon input

from the calculation of the equilibrium diagram. It has thus been demonstrated that the Gibbs energy functions describing the equilibrium phase diagram can be useful in deriving metastable as well as stable phase formation, and a complete assessment of the metastable equilibria should include consideration of equilibrium thermodynamic functions as well as kinetic factors.

LITERATURE SITED

Kubaschewski O., Iron Binary Phase Diagrams, Spring-Verlag, Berlin (1982)

Miedema A. R., F. R. De Boer, R. Boom and J. W. F. Dorleijn, Calphad 11, 341 (1977)

Miedema A. R. and A. K. Niessen, Calphad 7, 27 (1983)

Niessen A. K., F. R. De Boer, R. Boom, P. F. De Chatel, W. C. M. Mattens and A. R. Miedema, Calphad 7, 51 (1983)

Polk D. E. and B. C. Giessen, Metallic Glasses (ASM, Metals Park, Ohio, 1978)

ACKNOWLEDGMENTS

I wish to express my sincere appreciation to Dr. J. F. Smith for his guidance and encouragement during this study.

The author is also indebted to Ames Laboratory for use of the computer.

The financial assistance of the NBS and the Engineering Research Institute of Iowa State University is gratefully acknowledged.

Finally, the author would like to acknowledge the patience and understanding of his wife, Mi Kyung, and parents throughout this work.